RSC Advances

The effect of A-site doping in strontium palladium perovskite and its applications for non-enzymatic glucose sensing

Journal:	*RSC Advances*
Manuscript ID	RA-ART-11-2015-024107.R2
Article Type:	Paper
Date Submitted by the Author:	29-Jan-2016
Complete List of Authors:	El-Ads, Ekram; Faculty of Science, University of Cairo, Egypt, Department of Chemistry Galal, Ahmed; Cairo University, Faculty of Science, Chemistry; Kuwait University Faculty of Science, Chemistry Atta, Nada; Faculty of Science, University of Cairo, Egypt, Department of Chemistry
Subject area & keyword:	Electrochemistry < Physical

The effect of A-site doping in strontium palladium perovskite and its applications for non-enzymatic glucose sensing

Ekram H. El-Ads[1], Ahmed Galal[1,2], Nada F. Atta[*1]
[1]Chemistry Department, Faculty of Science, Cairo University, 12613 Giza, Egypt
E-mail address: anada@sci.cu.edu.eg, Phone: 0020235676561
[2]Chemistry Department, Faculty of Science, Kuwait University, Safat–13060, Kuwait

Abstract

The catalytic activity of strontium palladium perovskites, Sr_2PdO_3, toward non-enzymatic glucose sensing is strongly affected by the Sr^{2+} A-site partial substitution by Ca^{2+} ions; $Sr_{2-x}Ca_xPdO_3$ with x= 0–0.7. Scanning and transmission electron microscopies (SEM, EDAX and TEM), XRD, XPS, BET and particle size analyzer were used to investigate the microstructure, morphology, physical–chemical and electrochemical properties of the prepared perovskites. Well-crystalline orthorhombic Sr_2PdO_3 phase was formed as the main phase in all the prepared samples with particles size in the range of nanometers as confirmed by XRD. Doping the A-site Sr^{2+} cations with Ca^{2+} ions in Sr_2PdO_3 perovskite leads to the enhancement of the elecrocatalytic activity towards non-enzymatic glucose sensing showing the highest elecrocatalytic activity in case of $Sr_{1.7}Ca_{0.3}PdO_3$. This may be attributed to the higher free volume in the crystal lattice, enhanced content and mobility of surface lattice oxygen and distorted stabilized perovskite structure leading to higher catalytic activity of the prepared perovskites. In addition, synergistic interactions were achieved between Sr^{2+} and Ca^{2+} in the A-site and Pd^{2+} ions in the B-site resulted in improved surface activity and stabilized structure. As a result, greater ionic and electronic conductivity and enhanced catalytic activity were achieved upon doping. Graphite/$Sr_{1.7}Ca_{0.3}PdO_3$ as a free enzymatic glucose sensor exhibited good stability, low detection limit, high sensitivity, good selectivity even in presence of common interferents, applicability in real sample analysis and anti-interference ability.

Keywords: Ca-doped Sr_2PdO_3 perovskite; Catalytic activity; Synergistic interaction; Non-enzymatic glucose sensing; Selectivity.

1. Introduction

Glucose detection has great impact in many vital fields like biotechnology and clinical, food and pharmaceutical analyses [1, 2]. Patients with diabetes mellitus, one

of the major health afflictions worldwide, need to determine whether the treatments are effective by the regular measurement of blood glucose levels. As a result, the development of sensitive and selective glucose sensors is very crucial. Enzymatic glucose sensors suffer from some drawbacks like instability, complicated immobilization procedures, critical operating conditions and high cost of enzymes. Therefore, non-enzymatic glucose sensors have received great attention due to their high sensitivity, selectivity, good stability, high reliability, short response time, low cost and anti-fouling by enzyme-aging and adsorbed intermediates [1-8]. Several enzyme free glucose sensors have been constructed based on different strategies like metal nanoparticles such as CuS nanoflowers [9], Au [10-12], Ni nanoparticles [13] and Pt nanoflowers [8, 14], bimetallic nanostructures like dendritic Cu-Co nanostructures [7], binary Ni-Co hydroxide [5], Pt/Ni–Co nanowires [1] Ni and Cu nanoparticles [3] and AgNPs/CuO nanofibers [4], copolymer structures [6] and perovskite-type oxides like $LaNiO_3$ [2], $LaNi_{0.5}Ti_{0.5}O_3$ [15], $LaNi_{0.6}Co_{0.4}O_3$ [16], $La_{0.6}Sr_{0.4}FeO_{3-\delta}$ and $La_{0.6}Sr_{0}.4Co_{0.2}Fe_{0.8}O_{3-\delta}$ [17].

One of the potentially available materials for electrocatalytic oxidation of glucose is perovskite oxides; ABO_3 [2, 15, 16]. In the ABO_3 perovskites, the A-site metal in the body center is large cation surrounded by 12 oxygen ions with 12 coordination number and B- site metal in the three dimensional corner is smaller surrounded by 6 oxygen ions in the form of BO_6 octahedron with 6 coordination number [18-25]. As a result, the strong bonding between B-site ions and oxygen ions is the crucial character that determines the basic character of perovskite-type oxides [25]. A-site cation is responsible for the thermal resistance while B-site cation is responsible for the catalytic activity [19-24]. Perovskite oxides showed various physical and chemical characteristics like photocatalytic, magnetic, thermoelectric and dielectric properties, mixed ionic and electronic conductivity, electrically active structure, superconductivity, mobility of the oxide ions within the crystal, variations on the oxygen content, thermal and chemical stability, unique lattice oxygen chemistry and redox chemistry therefore they exhibited better catalytic activity for many reactions [24-27]. The redox ability and the oxygen defects of the perovskite oxides can be modified [27] and the cubic perovskite structure can be successfully stabilized [28] by partial substitution of different cations with different radii and charges in the A and/or B sites. They exhibited great tendency to accommodate a wide variety of cations on both the A and B sites demonstrating high degree of flexibility on composition,

structure and properties [29]. This can be achieved provided that the tolerance factor value *t* ranging between 0.75 and 1 and the electroneutrality are considered. The tolerance factor is used to investigate the structural stability and can be calculated from the following equation;

$t = (r_A + r_O) / ((r_B + r_O) \times 2^{0.5})$

Where r_A, r_B and r_O are the effective ionic radii of A- and B-site elements and oxygen ions, respectively [18, 28, 30, 31]. Additionally, the tolerance factor can be used as an indicator of the structural distortion of the perovskite structure from the ideal cubic perovskite structure which resulted from the misfit between different bond lengths. The electronic behavior of the perovskites is highly affected by their structural distortion level so that the tolerance factor is related to the physical properties of perovskites. Furthermore, the partial substitution of A- or B-site cations can result in cation vacancies distribution in the crystal lattice which affected greatly the perovskites properties [32]. Therefore, perovskite structure can host variable amounts of different lattice defects affecting greatly the perovskite activity and can stabilize the unusual valence states of different metal ions [30].

Furthermore, in the doped perovskites $A_{1-x}M_xBO_3$, the substitution of the A-site cation with various metal M ions affected greatly the crystal structure and the physical, electronic, optical and catalytic properties of the prepared perovskite [26, 33-40]. A-site doping resulted in the improvement of the flexible physical and chemical properties, catalytic activity and ionic and electronic conductivity of the prepared perovskite. Partial substitution of trivalent A-site cation like La^{3+} with bivalent cations of a lower oxidation state like Ca^{2+} or Sr^{2+}, which acts as electron acceptor on the A-site, resulted in the formation of oxygen vacancies and/or formation of a fraction of B cation in a higher valence state. In addition, higher free volume in the crystal lattice, enhanced content and mobility of surface adsorbed lattice oxygen and stabilized perovskite structure can be obtained. These achievements lead to greater ionic conductivity and enhanced catalytic activity of the doped perovskites [36-38, 24, 26, 27, 41-45]. On the other hand, doping the A-site with cation of the same oxidation state but with smaller ionic radius leads to distorted stabilized perovskite structure with three dimensional networks of the BO_6 octahedra and variation of the B–O–B bond angle and B–O bond length which further leads to higher catalytic activity of prepared perovskites [46].

Galal et al. proved that doping the A-site of $SrRuO_3$ with Ca^{2+} clearly enhanced the catalytic activity toward the hydrogen evolution reaction compared to the undoped one. The presence of two different metal ions (Sr^{2+} and Ca^{2+}) in the A-site enhanced the interaction between the A and B metal ions (synergistic interaction) and improved the surface area and the structure stability of the prepared materials. In addition, the catalytic activity of the prepared perovskite increased by increasing the fraction of Ca-doped because of the increased surface area and the enhanced structure stability [19]. Atta et al. proved the catalytic activity of strontium palladium perovskite in various applications like hydrogen evolution reaction catalysis [20] and neurotransmitters sensing [22, 23]. Strontium palladium perovskite showed low catalytic activity toward glucose sensing [21] which can be further improved upon its modification with gold nanoparticles. No one before explained the effect of A-site doping with Ca^{2+} in strontium palladium perovskite on the catalytic activity toward non-enzymatic glucose sensing.

This work focuses on Ca-doped strontium palladium perovskites with different amounts of Ca^{2+} = 0–0.7. One of the objectives of this study is to illustrate the effect of replacement of Sr^{2+} with different amounts of Ca^{2+} in the A-site of strontium palladium perovskite on the structural and catalytic properties, particularly the electrocatalytic activity in non-enzymatic glucose sensing. Ca-doped strontium palladium perovskites with various substitution degrees were prepared via glycine-nitrate combustion method and the preparation conditions and the amount and type of dopant were optimized. To the best of our knowledge, there is no structural studies or applications of Ca-doped strontium palladium perovskite mentioned in the literature. Doping the Sr^{2+} A-site in strontium palladium perovskite with Ca^{2+} resulted in improved conductivity and enhanced electrocatalytic activity when compared to the parent strontium palladium perovskite. The structure of the prepared Ca-doped strontium palladium perovskite was further investigated using XRD, XPS, SEM, EDAX, TEM and BET. Enhanced electrocatalytic activity towards non-enzymatic glucose sensing was achieved when using 0.3 moles of Ca compared to other ratios (0, 0.1, 0.5, 0.7). In addition, utilization of Ca^{2+} ions as a dopant in strontium palladium perovskite showed greater conductivity and higher electrocatalytic activity compared to other dopants (Mg^{2+}, Ba^{2+}). Ca^{2+} dopant enhanced the electronic properties of strontium palladium perovskite and facilitated the electron transfer rate.

The proposed non-enzymatic glucose sensor displayed good selectivity, high sensitivity, low detection limit and applicability in real samples.

2. Experimental

2.1. Materials

Potassium hexachloropalladate (IV) (K_2PdCl_6) (99.99%), strontium (II) nitrate ($Sr(NO_3)_2$) (99.995%), calcium nitrate ($Ca(NO_3)_2$), magnesium nitrate ($Mg(NO_3)_2$), barium nitrate ($Ba(NO_3)_2$), glycine, nitric acid and ammonium hydroxide were used as received from (Aldrich). Glucose, dopamine (DA), uric acid (UA) and ascorbic acid (AA) were supplied by Aldrich Chem. Co. (Milwaukee, WI. USA). 0.1 M NaOH was employed as a supporting electrolyte. In order to study the pH effect, phosphate buffer solution PBS (1 M K_2HPO_4 and 1 M KH_2PO_4) of pH 2-13 was used and the pH was adjusted using 0.1 M H_3PO_4 and 0.1 M KOH.

2.2. Instruments

The electrochemical measurements were performed using a BAS-100B electrochemical analyzer (Bioanalytical Systems, BAS, West Lafayette, USA) equipped with a standard three-electrode/one compartment glass cell. The working electrode was graphite electrode (diameter: 2.75 mm) and the auxiliary electrode was a large surface area platinum electrode. All the potentials in the electrochemical studies were referenced to Ag/AgCl (4 M KCl saturated with AgCl) electrode. Gamry-750 instrument and a lock-in-amplifier connected to a personal computer were utilized to study the electrochemical impedance spectroscopy (EIS). The data analysis was provided with the instrument and applied non-linear least square fitting with Levenberg-Marquardt algorithm. The ac frequency used in all the experiments was between 0.1 Hz and 100 kHz with 10 mV amplitude as an excitation signal. The measurements were performed under potentiostatic control at certain potential values which were decided from the recorded cyclic voltammograms.

2.3. Perovskite characterization

Microstructure of the samples was investigated using Quanta FEG 250 instrument. EDAX coupled to SEM was used to analyze the composition of the prepared samples. High resolution transmission electron microscope (HR-TEM, Tecnai G20, FEI, Netherland, 200 kV, LaB_6 Gun) was utilized to characterize the size and microstrucure of the prepared perovskites. The particle size distribution was achieved using Zeta sizer nano series (Nano ZS), Malvern, UK, size range (nm): 0.6:6000 nm and zeta potential range: (-200 mV to 200 mV). XRD data analysis was achieved

using XPERT–PRO–PANalytical–Netherland. An Al Kα line was used as the excitation source. XPS analysis was performed using PHI-5300 ESCA spectrometer (PerkinElmer) with an energy analyzer working in the pass energy mode at 35.75 eV.

2.4. Preparation of Ca-doped strontium palladium perovskite and electrode preparation

A series of Ca-doped strontium palladium tertiary perovskite with different amounts of Ca "x" (x=0, 0.1, 0.3, 0.5 and 0.7) was prepared by mixing (1-x) mole of $Sr(NO_3)_2$, x mole of $Ca(NO_3)_2$, 1 mole of K_2PdCl_6 and 2 moles of glycine through glycine-nitrate method to study the effect of doping of A-site with Ca^{2+}. The calcination temperature was 750 ºC for 3 h, the pH was 2 and the used fuel was glycine [21-23]. 1 ml of DMF was added to 10 mg of the prepared materials and sonicated for 30 minutes until a homogeneous suspension was obtained. Graphite electrode was polished well and casted with 30 µL of the prepared suspension [21-23] and the electrode was left to dry.

2.5. Analysis of urine

Direct analysis of glucose in human urine samples was performed to investigate the applicability of the proposed method in real sample analysis. The matrix effect of real samples was reduced by diluting urine sample 400 times with 0.1 M NaOH. A 15 mM stock solution of glucose was used and prepared in 0.1 M NaOH. Standard additions were carried out from the glucose stock solution in 10 mL of diluted urine.

3. Results and discussion

3.1. Characterization of Ca-doped strontium palladium perovskite

3.1.1. XRD

Ca-doped strontium palladium perovskites (amount of Ca= 0, 0.1, 0.3, 0.5, 0.7) were prepared by glycine-nitrate combustion method and sintered for 3 h at 750 °C. The phase formation of the prepared materials was confirmed by XRD. In the prepared materials, the Sr and Ca atoms occupy the A-site while the Pd atoms occupy the B-site. The XRD of Ca-doped strontium palladium perovskites with different amount of Ca was shown in Figure 1 and the data were compared with the ICDD card of Sr_2PdO_3 (card number 01-075-2163). In our previous work [20-23], we used the ICDD card of $SrPdO_3$ (card number 00-025-0908) but it was deleted by ICDD and replaced by Sr_2PdO_3 (card number 01-075-2163). Also, although we started with 1 mole of $Sr(NO_3)_2$ and 1 mole of K_2PdCl_6 to prepare $SrPdO_3$ or (1-x) mole of $Sr(NO_3)_2$, x mole of $Ca(NO_3)_2$ and 1 mole of K_2PdCl_6 to prepare $Sr_{1-x}Ca_xPdO_3$, the

obtained perovskite phase was Sr_2PdO_3 or $Sr_{2-x}Ca_xPdO_3$, respectively. Strontium palladium or distrontium palladium perovskite, Sr_2PdO_3, is a superconducting material exhibiting a body-centered orthorhombic lattice structure as marked by ICDD [47]. Sr_2PdO_3 belongs to A_2BO_3 perovskite [48] and high T_c cuprate families and its prototype is Sr_2CuO_3 [49, 50]. It is apparent that the crystal structure of Sr_2PdO_3 and Sr_2CuO_3 perovskites is the same [47, 51]. Sr_2CuO_3 with an orthorhombic unit cell resembled an intergrowth of an oxygen-deficient perovskite layer with a SrO rock salt layer [52]. In Sr_2PdO_3, Pd^{2+} is surrounded by four coplanar (rectangular) oxygen atoms while Sr^{2+} ion is surrounded by seven nearest oxygen neighbors [47, 48, 53]. Furthermore, Sr_2PdO_3 contained corner-linked chains of PdO_4 squares along the a-axis similar to the one-dimensional structure in Sr_2CuO_3 [48, 54].

For the prepared perovskites to be structurally stable, the tolerance factor should be as close to 1 as possible [31]. The values of the ionic radii for the different ions are used according to Shannon et al [55]. The tolerance factor is closely related to the lattice structure and stability of perovskite [56]. The tolerance factor for all the prepared perovskites was close to unity. It was 1.324 in case of Sr_2PdO_3 which decreased to 1.310 and 1.290 in case of $Sr_{1.7}Ca_{0.3}PdO_3$ and $Sr_{1.3}Ca_{0.7}PdO_3$, respectively indicating the distortion in the lattice upon doping. In addition, the values of the tolerance factor for Ca-doped Sr_2PdO_3 perovskites are within the values reached for the parent Sr_2PdO_3. In other words, the distortion in the Sr_2PdO_3 lattice upon doping with Ca^{2+} wasn't large to destroy the orthorhombic structure of the lattice. Doping the Sr_2PdO_3 lattice with small amounts of Ca^{2+} caused slight distortion, enhanced the perovskite stability and improved the electronic properties of the Sr_2PdO_3 perovskite as will be discussed later.

In Figure 1, the major diffraction peak (110) matched well with the theoretical one confirming the formation of the orthorhombic Sr_2PdO_3. While the diffraction peak (210) was related to $SrPd_3O_4$ secondary phase [47]. The XRD of $Sr_{2-x}Ca_xPdO_3$ with x = 0, 0.1 and 0.3 showed Sr_2PdO_3 as a primary phase and $SrPd_3O_4$ as a secondary phase. While at x = 0.5 and 0.7, the secondary phase was $CaPd_3O_4$ besides the Sr_2PdO_3 primary phase. The structure of the resulting perovskites with different x values is orthorhombic similar to that of non-substituted one Sr_2PdO_3. No diffraction peaks were detected related to any phases containing Ca and no metallic Ca had been observed in the XRD of $Sr_{1.9}Ca_{0.1}PdO_3$ and $Sr_{1.7}Ca_{0.3}PdO_3$. This result confirmed the insertion of Ca as a dopant inside the crystalline structure in case of $Sr_{1.9}Ca_{0.1}PdO_3$

and $Sr_{1.7}Ca_{0.3}PdO_3$ samples [57-59]. On the other hand, the XRD of $Sr_{1.5}Ca_{0.5}PdO_3$ and $Sr_{1.3}Ca_{0.7}PdO_3$ samples showed $CaPd_3O_4$ as a secondary phase besides the primary Sr_2PdO_3 phase. The formation of $CaPd_3O_4$ phase revealed that Ca was partly consumed in the formation of this phase. Therefore, the possibility of insertion of Ca^{2+} in the perovskite lattice decreased in case of $Sr_{1.5}Ca_{0.5}PdO_3$ and $Sr_{1.3}Ca_{0.7}PdO_3$ samples which may be the reason of the decrease in the catalytic activity of these samples. All the synthesized perovskites contained Sr_2PdO_3 as a primary phase regardless of the amount of Ca dopant. However, the percent of the primary phase and the ratio of the relative intensities of primary Sr_2PdO_3 peak and secondary $SrPd_3O_4$ or $CaPd_3O_4$ peak depend on the amount of Ca dopant (x). The order of decreasing the percent of primary phase was; $Sr_{1.7}Ca_{0.3}PdO_3$ > $Sr_{1.9}Ca_{0.1}PdO_3$ > Sr_2PdO_3 > $Sr_{1.5}Ca_{0.5}PdO_3$ > $Sr_{1.3}Ca_{0.7}PdO_3$. $Sr_{1.7}Ca_{0.3}PdO_3$ showed higher peak intensity revealing higher percent of the primary phase and higher crystallinity. Also, the order of decreasing the ratio of the relative intensities of primary Sr_2PdO_3 peak (110) and secondary $SrPd_3O_4$ or $CaPd_3O_4$ peak (210) was; $Sr_{1.7}Ca_{0.3}PdO_3$ > $Sr_{1.9}Ca_{0.1}PdO_3$ > $Sr_{1.5}Ca_{0.5}PdO_3$ > Sr_2PdO_3 > $Sr_{1.3}Ca_{0.7}PdO_3$. $Sr_{1.7}Ca_{0.3}PdO_3$ showed the highest percent of the primary phase and the highest ratio of the relative intensities of primary and secondary phases suggesting its perfect electronic properties and catalytic activity. This conclusion will be further confirmed with the morphology study and its electrocatalytic activity toward non-enzymatic glucose sensing.

On the other hand, the catalytic activity of the prepared materials was highly affected by their crystal size. The crystal size calculated from Scherrer equation was 38.28 nm for Sr_2PdO_3 which decreased to 30.09 and 27.26 nm in case of $Sr_{1.9}Ca_{0.1}PdO_3$ and $Sr_{1.7}Ca_{0.3}PdO_3$, respectively (Table 1). The crystallites of the perovskites phase have sizes in the range of 27.26 nm to 50.45 nm. The crystal size decreased upon doping the Sr^{2+} A-site with Ca^{2+} as Ca^{2+} (r = 1.07 °A) has smaller ionic radius than Sr^{2+} (r = 1.21 °A) [55] resulting in higher free volume in the unit cell and promoting oxygen ion mobility [38]. Some structural parameters like lattice parameters, lattice volume and theoretical density were calculated from XRD data and shown in Table 1. The lattice parameters values were comparable with that of the standard in case of $Sr_{1.9}Ca_{0.1}PdO_3$ and $Sr_{1.7}Ca_{0.3}PdO_3$ and therefore the values of lattice volume and the theoretical density were comparable with that of standard. In case of $Sr_{1.5}Ca_{0.5}PdO_3$ and $Sr_{1.3}Ca_{0.7}PdO_3$, there is a slight deviation in the values of lattice parameters compared to that of standard resulting in a slight deviation in the lattice volume and

the theoretical density compared to the standard. This may be attributed to the slight distortion in the orthorhombic lattice of the perovskite upon doping with higher amount of Ca (x= 0.5 and 0.7). The crystal lattice volume was 179.98, 179.63 and 179.06 $A^{\circ 3}$ in case of standard Sr_2PdO_3, $Sr_{1.9}Ca_{0.1}PdO_3$ and $Sr_{1.7}Ca_{0.3}PdO_3$, respectively. While it decreased slightly to 178.88 and 177.50 $A^{\circ 3}$ in case of $Sr_{1.5}Ca_{0.5}PdO_3$ and $Sr_{1.3}Ca_{0.7}PdO_3$, respectively.

In addition, the type of the dopant was studied and various alkaline earth metals were used in the synthesis of $Sr_{1.7}M_{0.3}PdO_3$ (M; Mg^{2+} with ionic radius 0.89 A° and Ba^{2+} with ionic radius 1.39 A°) [55]. XRD was used to confirm the structure of the prepared materials. There is a close matching between the primary diffraction peak (110) related to orthorhombic Sr_2PdO_3 and (210) related to $SrPd_3O_4$ secondary phase with the theoretical ones (Supplement Figure 1). Table 1 summarized the structural parameters like tolerance factor, crystal size, lattice parameters, lattice volume and theoretical density calculated from XRD data. There is a deviation in the values of lattice parameters resulting in an obvious deviation in the lattice volume and the theoretical density compared to the standard. This may be due to the observable distortion in the orthorhombic lattice of the perovskite upon doping with Mg^{2+} and Ba^{2+} resulting in decreased electrocatalytic activity toward non-enzymatic glucose sensing as we will show later.

Insert Figure 1 and Table 1

3.1.2. Surface area measurement

The electrochemical performance of the doped mixed oxides is related to the specific surface area of the materials [59] therefore it is important to measure the specific surface area of the prepared materials. The BET specific surface area of Sr_2PdO_3 was 8 m^2/g but upon doping with Ca, the BET specific surface area was about 2.5 m^2/g. The total pore volume was 1.532×10^{-2} cm^3/g and 9.685×10^{-3} cm^3/g in case of Sr_2PdO_3 and $Sr_{1.7}Ca_{0.3}PdO_3$, respectively. Extremely high electrocatalytic activity was observed toward glucose sensing at $Sr_{1.7}Ca_{0.3}PdO_3$ compared to Sr_2PdO_3 and other doped ratios of $Sr_{2-x}Ca_xPdO_3$ although the BET specific surface area of $Sr_{1.7}Ca_{0.3}PdO_3$ was lower than that of Sr_2PdO_3. This indicated that the doping of Sr_2PdO_3 with Ca^{2+} was favorable of creating more lattice defects and these lattice defects instead of surface area were mainly responsible for the high electrocatalytic activity of $Sr_{1.7}Ca_{0.3}PdO_3$ [36]. This indicated that the intrinsic surface area was not the only parameter affecting the electrocatalytic activity of the prepared materials.

3.1.3. Morphology

The porosity, particle size and edges of perovskite crystals affected greatly the catalytic activity of the prepared materials. The SEM of Sr_2PdO_3 and $Sr_{1.7}Ca_{0.3}PdO_3$ were shown in Figure 2 (A, B), respectively. The SEM of Sr_2PdO_3 and $Sr_{1.7}Ca_{0.3}PdO_3$ with greater magnification were shown in Supplement Figure 3 (A, B), respectively. The SEM of both perovskite materials showed clusters of particles rather than single separated ones due to the agglomeration of the crystals over the graphite surface. Perovskite crystals were embedded over graphite surface in both cases. Both Sr_2PdO_3 and $Sr_{1.7}Ca_{0.3}PdO_3$ crystals were homogenous in size and shape and well-distributed over the surface.

EDAX measurements were utilized to confirm the insertion of Ca in the prepared materials and confirm its amount. Figure 2 (C, D) showed the EDAX of Sr_2PdO_3 and $Sr_{1.7}Ca_{0.3}PdO_3$, respectively. The EDAX of Sr_2PdO_3 contained only Sr, Pd and O but the EDAX of $Sr_{1.7}Ca_{0.3}PdO_3$ contained Sr, Ca, Pd and O. These results confirmed the doping of Sr_2PdO_3 perovskite lattice with Ca^{2+} ions. Furthermore, we can confirm the atomic percent of Ca dopant and compare it with its real value. The atomic percent of Ca obtained from EDAX was 4.4 % which is close to its value in $Sr_{1.7}Ca_{0.3}PdO_3$ (5%) as the atomic percents of Sr, Ca, Pd and O in $Sr_{1.7}Ca_{0.3}PdO_3$ were 28.3%, 5%, 16.6% and 50%, respectively. Also, it was comparable with the real value of Ca in the preparation precursor we started with (6%). At this stage, it is reasonable to assume that Ca^{2+} has substituted for Sr^{2+} in this sample. This result confirmed the conclusion derived by the XRD that Ca in case of $Sr_{1.7}Ca_{0.3}PdO_3$ was completely inserted in the perovskite lattice. On the other hand, the atomic percents of Sr, Pd and O in $Sr_{1.7}Ca_{0.3}PdO_3$ obtained from EDAX were 10.1%, 24.7% and 60.8%, respectively. They were comparable to the actual percents we started with in the preparation precursor (14%, 20% and 60%, respectively). However, we started with 1 mole of $Sr(NO_3)_2$ and 1 mole of K_2PdCl_6 to prepare $SrPdO_3$ and 0.7 mole of $Sr(NO_3)_2$, 0.3 mole of $Ca(NO_3)_2$ and 1 mole of K_2PdCl_6 to prepare $Sr_{0.7}Ca_{0.3}PdO_3$, the obtained perovskite phases were Sr_2PdO_3 and $Sr_{1.7}Ca_{0.3}PdO_3$, respectively. The obtained data in EDAX was closely matched with the real values we started with. But these values are different from the atomic percents of Sr, Pd and O in $Sr_{1.7}Ca_{0.3}PdO_3$ (28.3%, 16.6% and 50%). This may be due to the other phases formed with Sr_2PdO_3 or $Sr_{1.7}Ca_{0.3}PdO_3$ like $SrPd_3O_4$.

TEM images of Sr_2PdO_3 and $Sr_{1.7}Ca_{0.3}PdO_3$ were shown in Fig. 2 (E, F), respectively. The XRD data of Sr_2PdO_3 and $Sr_{1.7}Ca_{0.3}PdO_3$ listed in section **3.1.1** was confirmed by

TEM diffraction patterns (Supplement Figure 3). The catalytic activity of the prepared perovskites was affected greatly by TEM textures in terms of distortion in shape, edges, roughness and defects. Twin and multi-crystals with ideal and distorted orthorhombic structure was shown in the TEM of Sr_2PdO_3. Also, the grains look to be rather clustered than described to be of larger size. On the other hand, the TEM of $Sr_{1.7}Ca_{0.3}PdO_3$ showed more edges imparting higher surface activity. It showed more cubic and prismatic structure with twin crystals. Also, there is a good consistency in the shape of the crystals. As well as, particles with smaller size in the range of 8-16 nm clearly appeared in case of $Sr_{1.7}Ca_{0.3}PdO_3$ but in case of Sr_2PdO_3 the size range was 15-29 nm. Smaller size of crystals, more edges and higher consistency in the crystals shape resulted in higher catalytic activity in case of $Sr_{1.7}Ca_{0.3}PdO_3$ compared to Sr_2PdO_3.

Furthermore, the particle size distribution was performed for Sr_2PdO_3 and $Sr_{1.7}Ca_{0.3}PdO_3$. The calculated particle diameter is about 639.1 nm and 232.3 nm for Sr_2PdO_3 and $Sr_{1.7}Ca_{0.3}PdO_3$, respectively (Supplement Figure 4). Due to the similar charges of the particles, their agglomeration takes place and resulted in large particles size for the studied cases. Therefore, this analysis gives an apparent description of the particle size distribution.

Insert Figure 2

3.1.4. XPS

The presence of dopants in the doped perovskites and the identification of their position within the crystal lattice were confirmed by XPS [30, 60]. XPS analysis was conducted as a part of structural characterizations of Sr_2PdO_3 and $Sr_{1.7}Ca_{0.3}PdO_3$ in order to get a detailed examination of the surface element compositions, the different oxidation states of A- and B-site metal ions and the nature of the adsorbed oxygen species. The XPS spectra of Sr(3d), Pd(3d) and O(1s) and Sr(3d), Pd(3d), O(1s) and Ca(2P) in Sr_2PdO_3 and $Sr_{1.7}Ca_{0.3}PdO_3$ were shown in Figure 3 (A, B), respectively. The XPS of Sr3d in Sr_2PdO_3 contains a doublet corresponding to $Sr3d_{3/2}$ and $Sr3d_{5/2}$ lines with binding energies at 136.19 and 134.34 eV, respectively. Only one peak for Sr3d appeared at 133.19 eV in case of $Sr_{1.7}Ca_{0.3}PdO_3$. The binding energy values of Sr(3d) in the two cases represented Sr^{2+} ions in perovskite oxide form [61]. In addition, the binding energy values of Sr(3d) in the two cases represented Sr^{2+} ions the form of Sr_2CuO_3 which matched the structure of Sr_2PdO_3 [47] according to the explanation derived by the NIST XPS standard reference database. The binding

energy value in case of $Sr_{1.7}Ca_{0.3}PdO_3$ represented Sr^{2+} ions in the form of $Bi_2Sr_2Ca_2Cu_3O_x$ indicating that Sr^{2+} ions was bonded to Ca^{2+} ions according to the NIST XPS standard reference database. The XPS of Pd(3d) showed a doublet at 342.24 and 336.88 eV for $3d_{3/2}$ and $3d_{5/2}$, respectively in case of Sr_2PdO_3 which are shifted to 343.06 and 337.75 eV, respectively in case of $Sr_{1.7}Ca_{0.3}PdO_3$. No peaks were reported at 335.2 eV for metallic Pd in both samples which confirmed that Pd was enclosed in the perovskite crystal lattice [62, 63]. From the values of binding energy of Pd(3d) in both samples, it was revealed that Pd^{2+} was included in the oxide form corresponding to Sr_2PdO_3 or $Sr_{1.7}Ca_{0.3}PdO_3$ as primary phase and $SrPd_3O_4$ as secondary phase. There is a slight shift in the values of binding energy of Sr(3d) and Pd(3d) upon doping with Ca^{2+} ions in $Sr_{1.7}Ca_{0.3}PdO_3$ from that in case of Sr_2PdO_3. Doping the Sr^{2+} A-site with Ca^{2+} which has smaller ionic radius resulted in higher free volume in the crystal lattice, enhanced oxygen ion mobility, increased surface lattice oxygen, higher conductivity and stabilized perovskite structure which resulted in higher electrocatalytic activity toward non-enzymatic glucose sensing compared to undoped samples [24, 26, 27, 36-38, 41-45]. Furthermore, the XPS of O(1s) in Sr_2PdO_3 showed a peak at 531.94 eV and a broad shoulder peak at 533.77 eV. In case of $Sr_{1.7}Ca_{0.3}PdO_3$, the XPS of O(1s) showed a peak at 531.14 eV and a broad shoulder peak at 535.04 eV. The peak with a low binding energy in both samples appeared at 531.94 eV and 531.14 eV resulted from the surface lattice oxygen species in the form of O^{2-} ion of the metal oxide [64]. The other one with a high binding energy in both cases appeared at 533.77 eV and 535.04 eV was attributed to the adsorbed oxygen species which may exist in oxygen vacancies of such defect oxides [30, 60, 61]. Upon doping with Ca^{2+} ions, the binding energy values related to surface lattice oxygen of $Sr_{1.7}Ca_{0.3}PdO_3$ are slightly lower than that of undoped Sr_2PdO_3. This means that the dopant ion has minor effect on peak position shifting the oxygen peaks to lower binding energies [61]. Furthermore, the percent amount of adsorbed oxygen species in oxygen vacancies (corresponding to binding energy at 533.77, 535.04 eV in Sr_2PdO_3 and $Sr_{1.7}Ca_{0.3}PdO_3$, respectively) was nearly the same which means that doping the A-site with Ca has no effect on the adsorped oxygen amount in oxygen vacancies. On the other hand, the percent amount of surface lattice oxygen (corresponding to binding energy at 531.94 eV and 531.14 eV in Sr_2PdO_3 and $Sr_{1.7}Ca_{0.3}PdO_3$, respectively) increased upon doping with Ca. These results indicated that the content and mobility of surface lattice oxygen were enhanced upon doping [60]. Therefore,

$Sr_{1.7}Ca_{0.3}PdO_3$ showed higher electrocatalytic activity toward non-enzymatic glucose sensing compared to undoped samples. In addition, the binding energy values of O(1s) in case of Sr_2PdO_3 represented O^{2-} ion in the perovskite phase while in case of $Sr_{1.7}Ca_{0.3}PdO_3$ represented O^{2-} ion in doped perovskite form according to the NIST XPS standard reference database. On the other hand, the XPS of Ca(2p) in $Sr_{1.7}Ca_{0.3}PdO_3$ showed a doublet at 346.70 eV and 350.28 eV corresponding to $2p_{3/2}$ and $2p_{1/2}$, respectively. They were ascribed to ionic calcium species Ca^{2+} attached to other metal ions like Sr^{2+} ($Bi_2Sr_2Ca_2Cu_3O_x$), oxygen O^{2-} or halide ions according to the NIST XPS standard reference database. The binding energy of metallic Ca was 346.57 eV which is lower than the observed value suggesting that Ca^{2+} ions were doped into the crystal lattice of Sr_2PdO_3 to produce $Sr_{1.7}Ca_{0.3}PdO_3$.

Insert Figure 3

3.2. Catalytic performance toward non-enzymatic glucose sensing

Doping the A and/or B sites with different metal ions affected remarkably the electronic and transport properties and catalytic activity of perovskites [65]. Doping the A-site of Sr_2PdO_3 with Ca^{2+} had a great effect on the electrocatalytic activity of the prepared materials toward free-enzymatic glucose sensing. The electrochemistry of 5 mM glucose/0.1 M NaOH at bare graphite, graphite/Sr_2PdO_3 and graphite/$Sr_{1.7}Ca_{0.3}PdO_3$ was shown in Figure 4A. The oxidation peak potential of glucose was at –135 mV, –61 mV and –77 mV with oxidation peak current of 5.30×10^{-5} A, 7.80×10^{-5} A and 6.92×10^{-4} A at bare graphite, graphite/Sr_2PdO_3 and graphite/$Sr_{1.7}Ca_{0.3}PdO_3$, respectively (Table 2). The increase in the anodic peak current of glucose was 1.5 and 13 folds upon modification with Sr_2PdO_3 and $Sr_{1.7}Ca_{0.3}PdO_3$, respectively compared to bare graphite electrode. This enhancement in the peak current reflected the high electrocatalytic activity of $Sr_{1.7}Ca_{0.3}PdO_3$ toward non-enzymatic glucose sensing. On the other hand, the effect of dopant amount on the electrocatalytic activity of the proposed graphite/$Sr_{2-x}Ca_xPdO_3$ (x = 0 - 0.7) toward non-enzymatic glucose sensing was studied. The inset of Figure 4A showed the relationship between the dopant concentration and the anodic peak current of glucose exhibiting a volcano shape with a maximum at x= 0.3. Upon doping with Ca^{2+} ions, the anodic peak current of glucose increased reaching a maximum value at x= 0.3 then decreased again at higher values. The anodic peak potentials of glucose were –61 mV, –77 mV and +22 mV with anodic peak currents of 7.8038×10^{-5} A, 6.9248×10^{-4} A and 4.0316×10^{-4} A at Sr_2PdO_3, $Sr_{1.7}Ca_{0.3}PdO_3$ and $Sr_{1.3}Ca_{0.7}PdO_3$, respectively (Table

2). The anodic peak current of glucose increased by ~ 9 folds at $Sr_{1.7}Ca_{0.3}PdO_3$ compared to Sr_2PdO_3 indicating the role of Ca^{2+} ions dopant in the enhancement of the electronic properties of Sr_2PdO_3 and mediation of charge transfer rate. The perovskitic oxides showed electrocatalytic activity toward glucose oxidation due to the presence of the transition metal ions with partially occupied d orbitals acting as active sites and resulting in deficiency of the surface for oxygen [56, 66, 67]. In addition, $Sr_{1.7}Ca_{0.3}PdO_3$ displayed fascinating electrocatalytic activity and stability toward glucose sensing. Doping the Sr^{2+} with Ca^{2+} resulted in higher free volume in the crystal lattice and enhanced content and mobility of surface lattice oxygen. It may also result in distorted stabilized perovskite structure which further leads to higher catalytic activity of prepared perovskites [46]. In addition, the presence of two different metal ions in the A-site (Sr^{2+}, Ca^{2+}) enhanced the interaction between the A and B metal ions (synergistic interaction) and improved the surface activity and the structure stability of the prepared materials [19]. These achievements lead to greater ionic and electronic conductivity and enhanced catalytic activity of the doped perovskites [24, 26, 27, 36-38, 41-45]. The optimum amount of Ca^{2+} ions used to improve the catalytic activity toward glucose sensing and enhancing the electrical conductivity of the prepared materials is x = 0.3. The enhanced catalytic activity and attracting properties of the prepared $Sr_{1.7}Ca_{0.3}PdO_3$ were confirmed before via XRD, SEM, TEM and XPS displaying the role of Ca^{2+} as a dopant. The glucose oxidation can be achieved through the chemisorption of glucose molecules at graphite/$Sr_{1.7}Ca_{0.3}PdO_3$ surface via dehydrogenation step at about –600 mV. Then, they were oxidized electrochemically through a 2-electron/2-proton step producing gluconolactone at –77 mV. At about +600 mV, a very broad peak was obtained due to the transformation of gluconolactone to gluconate.

Furthermore, the effect of the type of dopant ion was investigated as it affected remarkably the properties of the doped perovskites. In this study, we selected divalent cations like Mg^{2+} (0.89 A°), Ca^{2+} (1.07 A°) and Ba^{2+} (1.39 A°) to illustrate the effect of A-site dopant. The XRD analysis confirmed the formation of $Sr_{1.7}Mg_{0.3}PdO_3$, $Sr_{1.7}Ca_{0.3}PdO_3$ and $Sr_{1.7}Ba_{0.3}PdO_3$ (Supplement Figure 1). Figure 4B showed the CVs of 5 mM glucose/0.1 M NaOH at graphite/$Sr_{1.7}M_{0.3}PdO_3$ (M= Mg, Ca and Ba). The relation between the anodic peak current of glucose and the type of dopant was shown in the inset of Figure 4B. The highest current response was obtained in case of $Sr_{1.7}Ca_{0.3}PdO_3$ (Table 2). This may be attributed to the stronger interactions between

Sr^{2+}, Ca^{2+} and Pd^{2+}, higher surface activity, enhanced structure stability and greater ionic conductivity compared to the other two dopants. Upon doping with Mg^{2+} and Ba^{2+}, the electrocatalytic activity of $Sr_{1.7}M_{0.3}PdO_3$ (M= Mg and Ba) toward non-enzymatic glucose sensing decreased due to the great distortion in the orthorhombic lattice of the perovskite which affected the interaction between A and B-site metal ions. As a conclusion, the high catalytic activity of $Sr_{1.7}Ca_{0.3}PdO_3$ was attributed to higher free volume in the crystal lattice, enhanced content and mobility of surface lattice oxygen, stabilized distorted perovskite structure, enhanced synergistic interaction between the two different A cations and B metal ion and improved surface activity which further leads to greater electronic and ionic conductivity and higher catalytic activity of prepared perovskites.

The study of the scan rate effect can be used to further confirm the electrocatalytic activity of $Sr_{1.7}Ca_{0.3}PdO_3$ perovskite toward glucose sensing (5–100 mV s^{-1}) (Supplement Figure 5). The glucose oxidation at $Sr_{1.7}Ca_{0.3}PdO_3$ was controlled by diffusion as a result of the linear relationship between the anodic peak current and square root of the scan rate in the range of 5–100 mV s^{-1} (Supplement Figure 5). The linear regression equation was

I_{pa} (A) = $-5.962\times10^{-7} + 3.831\times10^{-3}\ \nu^{1/2}$ (V s^{-1})$^{1/2}$

The correlation coefficient is 0.9952. The apparent diffusion coefficient (D_{app}, $cm^2\ s^{-1}$) of glucose at $Sr_{2-x}Ca_xPdO_3$ (x = 0–0.7) was calculated from Randles Sevcik equation (Table 2). $Sr_{1.7}Ca_{0.3}PdO_3$ showed higher D_{app} value compared to the other ratios indicating its higher electrocatalytic activity. On the other hand, graphite/$Sr_{1.7}Ca_{0.3}PdO_3$ showed higher D_{app} ($1.878\times10^{-4}\ cm^2\ s^{-1}$) compared to the case of graphite/Sr_2PdO_3 ($2.385\times10^{-6}\ cm^2\ s^{-1}$) and bare graphite ($1.08\times10^{-6}\ cm^2\ s^{-1}$) demonstrating the role of Ca^{2+} ions as A-site dopant.

The electronic properties of the formed $Sr_{1.7}Ca_{0.3}PdO_3$ was affected by doping the Sr^{2+} (A site) with Ca^{2+} ions resulting in mediation of charge transfer at the electrode surface. In addition, the D_{app} for 5 mM glucose/ 0.1 M NaOH was calculated at graphite/$Sr_{1.7}M_{0.3}PdO_3$ (M = Mg, Ca and Ba). The highest D_{app} value was obtained at $Sr_{1.7}Ca_{0.3}PdO_3$ ($1.878\times10^{-4}\ cm^2\ s^{-1}$) compared to ($3.677\times10^{-5}\ cm^2\ s^{-1}$) in case of $Sr_{1.7}Mg_{0.3}PdO_3$ and ($2.737\times10^{-5}\ cm^2\ s^{-1}$) in case of $Sr_{1.7}Ba_{0.3}PdO_3$ due to the stronger synergistic interaction between Sr^{2+}, Ca^{2+} and Pd^{2+}, higher surface activity and greater ionic conductivity offering greater electrocatalytic activity in case of Ca. These results

clearly showed that the addition of Ca^{2+} dopant ions affected greatly the electrical conductivity and catalytic activity of Sr_2PdO_3.

Insert Figure 4 and Table 2

3.3. Chronocoulometry

Figure 5 showed the chronocoulometry (CC) experiments in 5 mM glucose/0.1 M NaOH at bare graphite, graphite/Sr_2PdO_3 and graphite/$Sr_{1.7}Ca_{0.3}PdO_3$. Inset of Figure 5 showed the CC experiments in glucose solution with different concentrations from 0 to 6 mM at graphite/$Sr_{1.7}Ca_{0.3}PdO_3$. The CC experiments were performed at two potential values recorded from the cyclic voltammetry (CV); the first value where is no oxidation of glucose takes place and the second value where the oxidation is complete [68]. D_{app} of glucose at different modified electrodes was calculated from Anson equation;

$Q = (2nFAC_{\circ}D^{1/2}t^{1/2}) /\pi^{1/2}$

Where A is the surface area of the electrode (0.0594 cm^2), $C_{\circ}$ is the concentration of glucose (5×10^{-6} mol cm^{-3}) and n is the number of electron transfer (= 2). The relation between Q (C) and $t^{1/2}$ ($s^{1/2}$) is linear and the slope of this line can be used to calculate D_{app} (cm^2 s^{-1}) of glucose. The slope of Anson plot in glucose was subtracted from the slope of the same experiment in absence of glucose and the resulting slope was used to calculate D_{app} [68]. The D_{app} values calculated from CC experiments were comparable with that calculated from cyclic voltammetry (Table 2). The order of decreasing D_{app} of glucose was (1.91×10^{-4} cm^2 s^{-1}) at graphite/$Sr_{1.7}Ca_{0.3}PdO_3$ > (2.526×10^{-6} cm^2 s^{-1}) at graphite/Sr_2PdO_3 > (1.27×10^{-6} cm^2 s^{-1}) at bare graphite. The previous trend confirmed the high catalytic activity of Ca-doped Sr_2PdO_3 and the role of Ca^{2+} ions in mediating the electron transfer rate.

Insert Figure 5

3.4. pH effect and OH^- ion concentration

The effect of changing the pH value on the response of $Sr_{1.7}Ca_{0.3}PdO_3$ in glucose solutions prepared in 0.1 M PBS of pH range (2.7- 12.5) was studied (Supplement Figure 6). The anodic peak potential was shifted to less positive value with increasing the pH demonstrating that the glucose oxidation is pH dependent. In addition, the anodic peak current reached its maximum value at pH 12.5 confirming the role of high pH value in the electrocatalytic oxidation of glucose. The carbohydrates oxidation was greatly improved at metallic electrodes in OH^- ions media [1, 4, 11]. As a result, the effect of different concentrations of NaOH from 0.01 M to 0.5 M was

investigated (Supplement Figure 7). The anodic peak current of glucose at $Sr_{1.7}Ca_{0.3}PdO_3$ increased with increasing NaOH concentration up to 0.1 M reaching a steady state at higher concentrations. Furthermore, the anodic peak potential of glucose at $Sr_{1.7}Ca_{0.3}PdO_3$ was shifted to more negative values with NaOH concentration. Therefore, 0.1 M NaOH was chosen for glucose determination at $Sr_{1.7}Ca_{0.3}PdO_3$ [1-3, 7, 11, 13, 15, 16, 21]. As a result, hydroxide-rich solution with 0.1 M concentration was chosen as an optimum medium for glucose electrocatalytic oxidation at $Sr_{1.7}Ca_{0.3}PdO_3$.

3.5. Selectivity of $Sr_{1.7}Ca_{0.3}PdO_3$ toward glucose

It is necessary to detect glucose in the presence of most common interfering species as ascorbic acid (AA), uric acid (UA) and dopamine (DA) to test the selectivity of the proposed non-enzymatic glucose sensor; graphite/$Sr_{1.7}Ca_{0.3}PdO_3$. The physiological concentrations of UA (0.1 mM) and AA (0.1 mM) were much lower than that of glucose (3–8 mM) [21]. Furthermore, chloride ions may cause poisoning of the sensor as it may cause blocking of the active sites at the surface of the sensor therefore it's necessary to check the effect of chloride ions on the response of the proposed sensor [21, 69]. The linear sweep voltammetric (LSV) behaviors of graphite/$Sr_{1.7}Ca_{0.3}PdO_3$ in a solution containing 5 mM glucose, 0.1 mM UA, 0.1 mM AA and 0.1 M NaCl/0.1 M NaOH were shown in Figure 6 (A). Furthermore, the same measurements for solutions containing 5 mM glucose, 0.05 mM DA and 0.1 M NaCl/0.1 M NaOH and 5 mM glucose and 0.1 M NaCl/0.1 M NaOH were shown in Figure 6 (B, C), respectively. The electrochemical response of the proposed sensor towards glucose remained almost constant even in presence or absence of interferents confirming the high selectivity of the proposed sensor. In addition, electrochemical response of the proposed sensor toward glucose was relatively constant in the presence of Cl^- ions demonstrating that the sensor doesn't suffer from any poisoning in the presence of Cl^- ions. The presence of Ca^{2+} ions as a dopant enhanced the intrinsic electronic properties of Sr_2PdO_3 which resulted in the good selectivity of graphite/$Sr_{1.7}Ca_{0.3}PdO_3$. The proposed non-enzymatic sensor is free from interference from the common interferents in the human body showing its real application for the sensitive and selective determination of glucose.

Insert Figure 6

3.6. Determination of glucose at $Sr_{1.7}Ca_{0.3}PdO_3$ and its applicability in human urine samples

The LSVs of standard additions of 15 mM glucose/0.1 M NaOH to 10 mL of 0.1 M NaOH at graphite/$Sr_{1.7}Ca_{0.3}PdO_3$ were shown in Figure 7. The relationship between glucose concentration and its anodic peak current values was linear in the range from 5 μM to 5.6 mM (Inset of Figure 7). The linear regression equation in the linear range of 5 μM to 1.4 mM was

I_{pa} (A) = 3.069×10^{-4} c (mM) + (3.699×10^{-5}) with correlation coefficient (r^2) = 0.9956, sensitivity = 306.9 μA/mM and detection limit of 0.0845 μM. While the regression equation in the linear range of 1.8 mM to 5.6 mM was

I_p (A) = 5.417×10^{-5} c (mM) + (4.346×10^{-4}) with r^2 = 0.9938, sensitivity = 54.17 μA/mM and detection limit of 0.479 μM. The following equation was used to calculate the detection limit (D L);

DL = 3 s⁄b

Where s is the standard deviation of the peak currents and b is the slope of the calibration curve. Supplement table 1 contained a comparison of the sensing performances of the proposed sensor; graphite/$Sr_{1.7}Ca_{0.3}PdO_3$ and previously reported non-enzymatic glucose sensor. As we can see from the table that graphite/$Sr_{1.7}Ca_{0.3}PdO_3$ showed good linear range, higher sensitivity (306.9 μA/mM which equivalent to 5166.7 μA/mM cm^2) and lower detection limit (0.0845 μM) compared to other non-enzymatic sensors reported in the literature resulting in perfect sensing performance.

Furthermore, $Sr_{1.7}Ca_{0.3}PdO_3$ was applied for the determination of glucose in human urine samples with high precision and accuracy. The calibration curve of glucose in urine in the linear range of 5 μM to 6 mM was achieved with detection limit of 0.202 μM and correlation coefficient of 0.9955. In addition, five different concentrations on the calibration curve were chosen and repeated to calculate the accuracy and precision of the proposed method (Table 3). Good recovery values were obtained in the range of 98.9 % to 100.9 % with relative standard deviation below 1.33 % indicating that these procedures are free from interferences of the urine sample matrix. As a result, $Sr_{1.7}Ca_{0.3}PdO_3$ can be used to determine glucose with good sensitivity, selectivity, reproducibility and low detection limit in real samples.

Insert Figure 7 and Table 3

3.7. Stability of the proposed sensor

One important parameter affecting the performance of any sensor is its stability. Graphite/$Sr_{1.7}Ca_{0.3}PdO_3$ showed excellent stability upon repeated cycling up to 50

cycles in 5 mM glucose/0.1 M NaOH (Inset 2 of Figure 8). In addition, $Sr_{1.7}Ca_{0.3}PdO_3$ exhibited highly stable current response upon amperometric studies in glucose at the oxidation (–70 mV) and steady state (250 mV) potentials (Figure 8 and Inset 1, respectively). Therefore, Graphite/$Sr_{1.7}Ca_{0.3}PdO_3$ was utilized as a long-term stable non-enzymatic glucose sensor.

Insert Figure 8

3.8. Electrochemical Impedance Spectroscopy

The EIS measurements were operated in a solution of 5 mM glucose/0.1 M NaOH at graphite/Sr_2PdO_3 and graphite/$Sr_{1.7}Ca_{0.3}PdO_3$ over 0.1-100 kHz ac frequency range at open circuit potential (OCP) and steady state potential. The Nyquist plots for graphite/Sr_2PdO_3 and graphite/$Sr_{1.7}Ca_{0.3}PdO_3$ at OCP and steady state potential are presented in Figure 9 and the inset, respectively. The equivalent circuit used in the fitting of the experimental data contained R_s; the solution resistance, R_p; the charge transfer resistance, C_f, C_p and C_d; the capacitances of the double layer, Z; the Warburg impedance due to diffusion and CPE1 and CPE2; the predominant diffusion influence on the charge transfer process and n1 and n2 its corresponding exponent. Table 4 showed the fitting values calculated from the equivalent circuit for the impedance data. Doping Sr_2PdO_3 with Ca^{2+} affected remarkably the impedance behavior of the prepared materials in glucose and the same impedance behavior was obtained at OCP and steady state potential. The Nyquist plot in case of Sr_2PdO_3 and $Sr_{1.7}Ca_{0.3}PdO_3$ contained linear portion at lower frequencies reflecting that the process is diffusion-controlled and semicircle portion at higher frequencies reflecting that the process is kinetic-controlled [22, 23]. The semicircle portion was with smaller diameter in case of $Sr_{1.7}Ca_{0.3}PdO_3$. The diameter of the semicircle represented the R_p which equaled 1329 Ω cm^2 in case of Sr_2PdO_3 and decreased to about 663.6 Ω cm^2 in case of $Sr_{1.7}Ca_{0.3}PdO_3$ at steady state potential and 3462 Ω cm^2 which decreased to 2623 Ω cm^2 at OCP, respectively. These results indicated that the electrochemical glucose oxidation is kinetically faster and the electron transfer rate was enhanced in case of $Sr_{1.7}Ca_{0.3}PdO_3$. Besides, there is a remarkable decrease in the value of Z in case of $Sr_{1.7}Ca_{0.3}PdO_3$ compared to Sr_2PdO_3 indicating enhanced diffusion and more mediation of charge transfer. On the other hand, the conducting character of Sr_2PdO_3 was enhanced upon doping with Ca^{2+} in $Sr_{1.7}Ca_{0.3}PdO_3$ as confirmed by the values of capacitances (C_f, C_p and C_d) in table 4. Therefore, doping the Sr^{2+} A-site of Sr_2PdO_3

with Ca^{2+} affected remarkably the electronic properties of $Sr_{1.7}Ca_{0.3}PdO_3$ and mediated the electron transfer rate.

Insert Figure 9 and table 4

4. Conclusions

The catalytic activity of Sr_2PdO_3 perovskites can be changed by partially substituted the A-site Sr^{2+} cations with Ca^{2+} cations. Doping the A-site Sr^{2+} cations with Ca^{2+} ions in Sr_2PdO_3 perovskite, $Sr_{2-x}Ca_xPdO_3$, resulted in the improvement of the electrocatalytic activity of Sr_2PdO_3 for non-enzymatic glucose sensing depending on the amount of Ca^{2+} dopant. $Sr_{1.7}Ca_{0.3}PdO_3$ perovskite showed the highest electrocatalytic activity toward non-enzymatic glucose sensing among all the prepared catalysts; $Sr_{2-x}Ca_xPdO_3$ with x= 0–0.7. The enhancement of the catalytic activity upon doping Sr_2PdO_3 perovskite with Ca^{2+} ions may be attributed to the higher free volume in the crystal lattice, enhanced content and mobility of surface lattice oxygen and distorted stabilized perovskite structure leading to higher catalytic activity of the prepared perovskites. In addition, synergistic interactions were achieved between the two different metal ions in the A-site and B metal ion which may result in improved surface activity and stabilized structure of the prepared materials. As a result, greater ionic and electronic conductivity and enhanced catalytic activity was achieved upon doping. In addition, the dependency of the electrical conductivity and catalytic activity of $Sr_{1.7}M_{0.3}PdO_3$ (M; Mg, Ca and Ba) toward non-enzymatic glucose sensing on the type of M dopant was clearly investigated demonstrating the highest electrocatalytic activity in case of $Sr_{1.7}Ca_{0.3}PdO_3$. This may be attributed to the stronger synergistic interactions between Sr^{2+}, Ca^{2+} in A-site and Pd^{2+} in B-site. The crystallinity of Sr_2PdO_3 is improved upon doping with Ca as revealed by XRD and TEM images. The proposed non-enzymatic glucose sensor, graphite/$Sr_{1.7}Ca_{0.3}PdO_3$, exhibited good performance in terms of long term stability, detection limit, sensitivity and selectivity even in presence of most common interferents. $Sr_{1.7}Ca_{0.3}PdO_3$ as a novel material has opened up new era of research in non-enzymatic glucose sensing.

5. Acknowledgment

The authors would like to acknowledge the financial support from Cairo University through the Vice President Office for Research Funds.

6. References

[1] S. S. Mahshid, S. Mahshid, A. Dolati, M. Ghorbani, L. Yang, S. Luo and Q. Cai, *J. Alloys Compd.*, 2013, **554**, 169–176.

[2] B. Wang, S. Gu, Y. Ding,Y. Chu, Z. Zhang, X. Ba, Q. Zhang and X. Li, *Analyst*, 2013, **138**, 362–367.
[3] K. Lin, Y. Lin and S. Chen, *Electrochim. Acta*, 2013, **96**, 164– 172.
[4] B. Zheng, G. Liu, A. Yao, Y. Xiao, J. Du, Y. Guo, D. Xiao, Q. Hu and M. M. F. Choi, *Sens. Actuators, B.*, 2014, **195**, 431–438.
[5] C. Lien, J. Chen, C. Hu and D. S. Wong, *J. Taiwan Inst. Chem. Eng.*, 2014, **45**, 846–851.
[6] Y. Chen, H. Zhang, H. Xue, X. Hu, G. Wang and C. Wang, *Mater. Sci. Eng., C*, 2014, **35**, 420–425.
[7] L. Wang, Y. Zheng, X. Lu, Z. Li, L. Sun and Y. Song, *Sens. Actuators, B.*, 2014, **195**, 1–7.
[8] X. Zhou, X. Zheng, R. Lv, D. Kong and Q. Li, *Electrochim. Acta*, 2013, **107**, 164–169.
[9] Y. J. Yang, J. Zi and W. Li, *Electrochim. Acta*, 2014, **115**, 126– 130.
[10] L. Yang, Y. Zhang, M. Chu, W. Deng, Y. Tan, M. Ma, X. Su, Q. Xie and S. Yao, *Biosens. Bioelectron.*, 2014, **52**, 105–110.
[11] G. Chang, H. Shu, K. Ji, M. Oyama, X. Liu and Y. He, *Appl. Surf. Sci.*, 2014, **288**, 524– 529.
[12] M. Gougis, A. Tabet-Aoul, D. Ma and M. Mohamedi, *Sens. Actuators, B.*, 2014, **193**, 363– 369.
[13] J. Yang, J. Yu, J. R. Strickler, W. Chang and S. Gunasekaran, *Biosens. Bioelectron.*, 2013, **47**, 530–538.
[14] G. Wu, X. Song, Y. Wu, X. Chen, F. Luo and X. Chen, *Talanta*, 2013, **105**, 379–385.
[15] Y. Wang, Y. Xu, L. Luo, Y. Ding, X. Liu and A. Huang, *Sens. Actuators, B.*, 2010, **151**, 65–70.
[16] Z. Zhang, S. Gu, Y. Ding and J. Jin, *Anal. Chim. Acta*, 2012, **745**, 112– 117.
[17] L. F. Liotta, F. Puleo, V. L. Parola, S. G. Leonardi, N. Donato, D. Aloisio and G. Neri, *Electroanalysis*, 2014, **27**, 1–10.
[18] D. Lybye, F. W. Poulsen and M. Mogensen, *Solid State Ionics*, 2000, **128**, 91–103.
[19] N. F. Atta, A. Galal and S. M. Ali, *Int. J. Electrochem. Sci.,* 2012, **7**, 725–746.
[20] A. Galal, N. F. Atta, S. A. Darwish, A. Abdel Fatah and S. M. Ali, *J. Power Sources*, 2010, **195**, 3806–3809.
[21] E. H. El-Ads, A. Galal and N. F. Atta, *J. Electroanal. Chem.*, 2015, **749**, 42.
[22] N. F. Atta, S. M. Ali, E. H. El-Ads and A. Galal, *Electrochim. Acta*, 2014, **128**, 16–24.
[23] N. F. Atta, S. M. Ali, E. H. El-Ads and A. Galal, *J. Electrochem. Soc.*, 2013, **160 (7)**, G3144-G3151.
[24] R. Li, C. Yu and S. Shen, *J. Nat. Gas Chem.*, 2002, **11**, 137-144.
[25] M. Oishi, K. Yashiro, K. Sato, J. Mizusaki and T. Kawada, *J. Solid State Chem.*, 2008, **181**, 3177–3184.
[26] H. J. Wei, Y. Cao, W. J. Ji and C. T. Au, *Catal. Commun.*, 2008, **9**, 2509–2514.
[27] C. Zhang, W. Hua, C. Wang, Y. Guo, Y. Guo, G. Lu, A. Baylet and A. Giroir-Fendler, *Appl. Catal., B*, 2013, **134–135**, 310–315.
[28] J. Sunarso, J. Motuzas, S. Liu and J. C. D. d. Costa, *J. Membr. Sci.*, 2010, **361**, 120–125.
[29] F. Lin and W. Shi, *Phys. B*, 2012, **407**, 451–456.
[30] M. Alifanti, R. Auer, J. Kirchnerova, F. Thyrion, P. Grange and B. Delmon, *Appl. Catal., B*, 2003, **41**, 71–81.

[31] Z. Yang, M. Han, P. Zhu, F. Zhao and F. Chen, *Int. J. Hydrogen Energy*, 2011, **36**, 9162–9168.
[32] L. Malavasi, C. Ritter, M. C. Mozzati, C. Tealdi, M. S. Islam, C. B. Azzoni and G. Flor, *J. Solid State Chem.*, 2005, **178**, 2042–2049.
[33] A. Srivastava, N. K. Gaur, N. Kaur and R. K. Singh, *J. Magn. Magn. Mater.*, 2008, **320**, 2596–2601.
[34] A. K. Eriksson, T. Tran, S. Saxin, G. Svensson, P. Svedlindh, S. Eriksson and C. Knee, *Solid State Sci.*, 2009, **11**, 1945–1954.
[35] S. Yan, Y. Chang, W. Hwang and Y. Chang, *J. Lumin.*, 2012, **132**, 1867–1872.
[36] K. J. Yoon, J. W. Stevenson and O. A. Marina, *J. Power Sources*, 2011, **196**, 8531– 8538.
[37] R. N. Singh and B. Lal, *Int. J. Hydrogen Energy*, 2002, **27**, 45–55.
[38] Z. Gong, X. Yin and L. Hong, *Solid State Ionics*, 2009, **180**, 1471–1477.
[39] S. B. Zhang, Y. P. Sun, B. C. Zhao, X. B. Zhu and W. H. Song, *Solid State Commun.*, 2006, **138**, 123–128.
[40] A. Petric and P. Huang, *Solid State Ionics*, 1996, **92**, 113-117.
[41] Y. Takahashi, A. Kawahara, T. Suzuki, M. Hirano and W. Shin, *Solid State Ionics*, 2010, **181**, 300–305.
[42] Z. Ma, X. Gao, X. Yuan, L. Zhang, Y. Zhu and Z. Li, *Catal. Commun.*, 2011, **12**, 817–821.
[43] S. Hong and G. Lee, *Catal. Today*, 2000, **63**, 397–404.
[44] A. Evdou, V. Zaspalis and L. Nalbandian, *Fuel*, 2010, **89**, 1265–1273.
[45] J. Suntivich, K. J. May, H. A. Gasteiger, J. B. Goodenough and Y. Shao-Horn, *Science*, 2011, **334**, 1383–1385.
[46] D. Liao, Y. Sun, R. Yang and Z. Cheng, *Phys. B*, 2007, **394**, 104–110.
[47] O. Miller and R. Roy, Synthesis and Crystal Chemistry of Some New Complex Palladium Oxides, Robert F. Gould Editor, Advances in Chemistry Series book, 158th Meeting of the American Chemical Society, New York, N. Y., Sept. 8-9, 1969.
[48] Y. Tsujimoto, K. Yamaura and E. Takayama-Muromachi, *Appl. Sci.*, 2012, **2**, 206–219.
[49] P. Villars, Springer & Material Phases Data System (MPDS), CH-6354 Vitznau, Switzerland & National Institute for Materials Science (NIMS), Springer Materials Sr_2PdO_3 Crystal Structure, Japan, 2014, Database name LINUS PAULING FILE Multinaries Edition – 2012, Dataset ID sd_0375642.
[50] P. Villars, K. Cenzual and R. Gladyshevskii, Hand book of inorganic substances, 2015. ISBN-13: 978-3110294453, ISBN-10: 3110294451
[51] M. A. Augustyniak-Jabłokowa, I. Jacyna-Onyszkiewiczb, T. A. Ivanovac, V. K. Polovniakd, V. A. Shustovc and Y. V. Yablokov, *Acta Phys. Pol., A*, 2008, **114 (1)**, 197–201.
[52] J. J. Zuckerman (Founding Editor), A. P. Hagen (Editor), Handbook of Inorganic Reactions and Methods, Formation of Bonds to O, S, Se, Te, Po, Part 2, ISBN: 978-0-471-24677-0, 536 pages, November 1998.
[53] T. Yamamoto, Synthesis, Structure, and Physical Properties of Novel Iron Oxides Prepared by Topotactic Reactions, 2012, Kyoto University. Doctoral degree report no. 17235.
[54] E. G. Tulsky and J. R. Long, *Chem. Mater.*, 2001, **13 (4)**, 1149-1166.
[55] R. D. Shannon and C. T. Prewitt, *Acta Crystal*, 1969, **B25**, 925–946.
[56] H. Inaba, H. Hayashi and M. Suzuki, *Solid State Ionics*, 2001, **144**, 99–108.
[57] N. Russo, P. Palmisano and D. Fino*, Chem. Eng. J.*, 2009, **154**, 137–141.

[58] G. R. O. Silva, J. C. Santos, D. M. H. Martinelli, A. M. G. Pedrosa, M. J. B. d. Souza and D. M. A. Melo, *Mater. Sci., Appl.*, 2010, **1**, 39–45.
[59] P. Zeng, R. Ran, Z. Chen, W. Zhou, H. Gu, Z. Shao and S. Liu, *J. Alloys Compd.*, 2008, **455**, 465–470.
[60] Z. Li, M. Meng, Q. Li, Y. Xie, T. Hu and J. Zhang, *Chem. Eng. J.*, 2010, **164**, 98–105.
[61] N. Lakshminarayanan, H. Choi, J. N. Kuhn1 and U. S. Ozkan, *Appl. Catal., B*, 2011, **103**, 318–325.
[62] C. Li, C. Wang and Y. Lin, *Catal. Today*, 2011, **174**, 135–140.
[63] Z. Ke-bin, C. Hong-de, T. Qun, Z. Bao-wei, S. Di-xin and X. Xiao-bai, *J. Environ. Sci.*, 2005, **17(1)**, 19–24.
[64] G. C. M. Rodríguez and B. Saruhan, *Appl. Catal., B*, 2010, **93**, 304–313.
[65] Y. Cao, B. Lin, Y. Sun, H. Yang and X. Zhang, *J. Alloys Compd.*, 2015, **624**, 31–39.
[66] F. Y. Liang, K. P. Amarloei, H. Q. Jiang, H. X. Luo and J. Caro, Leibniz University Hannover, Germany, Max Planck Institut fur Kohlenforschung, Germany.
[67] Z. Gong, X. Yin and L. Hong, *Solid State Ionics*, 2009, **180**, 1471–1477.
[68] N. F. Atta and M. F. El-Kady, *Talanta*, 2009, **79**, 639–647.
[69] X. Chen, Z. Lin, D. Chen, T. Jia, Z. Cai, X. Wang, X. Chen, G. Chen and M. Oyama, *Biosens. Bioelectron.*, 2010, **25**, 1803–1808.

List of Figures

Figure 1: XRD patterns of $Sr_{2-x}Ca_xPdO_3$ with x= 0, 0.1, 0.3, 0.5 and 0.7 prepared by glycine-nitrate combustion method. Miller indices (h, l, k) are written in black line for Sr_2PdO_3, red line for $SrPd_3O_4$, blue line for $CaPd_3O_4$, the black circle (0) for $SrCl_2.6H_2O$, the red circle (0) for KCl and blue circle (0) for $SrCO_3$.

Figure 2: SEM micrographs of **(A)** graphite/Sr_2PdO_3 and **(B)** graphite/$Sr_{1.7}Ca_{0.3}PdO_3$, with magnification 5,000×. The EDAX measurement for **(C)** graphite/Sr_2PdO_3 and **(D)** graphite/$Sr_{1.7}Ca_{0.3}PdO_3$. TEM micrographs of **(E)** Sr_2PdO_3 and **(F)** $Sr_{1.7}Ca_{0.3}PdO_3$.

Figure 3: XPS of Sr3d, Pd3d and O1s and Sr3d, Pd3d, O1s and Ca2p for **(A)** Sr_2PdO_3 and **(B)** $Sr_{1.7}Ca_{0.3}PdO_3$, respectively.

Figure 4: (A) CVs of 5 mM glucose/0.1 M NaOH at bare graphite, graphite/Sr_2PdO_3 and graphite/$Sr_{1.7}Ca_{0.3}PdO_3$, scan rate 50 mV s^{-1} and the inset; the relation between the amount of Ca dopant (x=0–0.7) and the anodic peak current of glucose at graphite/$Sr_{2-x}Ca_xPdO_3$. **(B)** CVs of 5 mM glucose/0.1 M NaOH at graphite/$Sr_{1.7}M_{0.3}PdO_3$ (M; Mg, Ca and Ba), scan rate 50 mV s^{-1} and the inset; the relation between the type of dopant and the anodic peak current of glucose.

Figure 5: Dependence of Q (mC) on t (s) in the chronocoulometric studies obtained at different modified electrodes; bare graphite, graphite/Sr_2PdO_3 and graphite/$Sr_{1.7}Ca_{0.3}PdO_3$ in 5 mM glucose/0.1 M NaOH. Inset; Dependence of Q (mC)

on t (s) in the chronocoulometric studies obtained at graphite/$Sr_{1.7}Ca_{0.3}PdO_3$ in 0.1 M NaOH for different concentrations of glucose 0–6 mM.

Figure 6: (A) LSVs of 5 mM glucose/0.1 M NaOH in the absence and the presence of 0.1 mM AA, 0.1 mM UA and 0.1 M NaCl at graphite/$Sr_{1.7}Ca_{0.3}PdO_3$.

(B) LSVs of 5 mM glucose/0.1 M NaOH in the absence and the presence of 0.05 mM DA and 0.1 M NaCl at graphite/$Sr_{1.7}Ca_{0.3}PdO_3$.

(C) LSVs of 5 mM glucose/0.1 M NaOH in the absence and the presence of 0.1 M NaCl at graphite/$Sr_{1.7}Ca_{0.3}PdO_3$.

Figure 7: Calibration curve for glucose for concentrations from (5 μM to 1.4 mM) and from (1.8 mM to 5.6 mM). Inset: LSVs of 10 ml of 0.1 M NaOH at graphite/$Sr_{1.7}Ca_{0.3}PdO_3$ in different concentrations of glucose (5 μM to 5.6 mM).

Figure 8: (A) Chronoamperogram of graphite/$Sr_{1.7}Ca_{0.3}PdO_3$ at the oxidation potential of glucose (–70 mV) in 5 mM glucose/ 0.1 M NaOH, inset (1), the same study at the steady state potential of glucose (250 mV) and inset (2), CVs of repeated cyclic stability of graphite/$Sr_{1.7}Ca_{0.3}PdO_3$ in 5 mM glucose/ 0.1 M NaOH, 50 repeated cycles, scan rate 50 mV s^{-1}.

Figure 9: Nyquist plot of graphite/$Sr_{1.7}Ca_{0.3}PdO_3$ (red circles) and graphite/Sr_2PdO_3 (black circles) in 5 mM glucose/0.1 M NaOH at open circuit potentials and the inset, at the steady state potential. (Symbols and solid lines represent the experimental measurements and the computer fitting of impedance spectra, respectively), frequency range: 0.1–100 000 Hz. Inset, the equivalent circuit used in the fit procedure of the impedance spectra.

Table 1: Structural parameters calculated from XRD data.

	Crystal Structure	**Lattice Parameters A°**	**Lattice Volume $A^{\circ 3}$**	**Theoretical density g/cm^3**	**Crystal size nm**	**Goldschmidt tolerance factor "*t*"**
Standard Sr_2PdO_3 card number (01-075-2163)	Orthorhombic	a = 3.977 b = 3.530 c = 12.820	179.98	4.47	---	---
Sr_2PdO_3 (x= 0)	Orthorhombic	a = 3.982 b = 3.550 c = 12.836	181.45	4.43	38.28	1.324
$Sr_{1.9}Ca_{0.1}PdO_3$ (x= 0.1)	Orthorhombic	a = 3.9762 b = 3.524 c = 12.818	179.63	4.47	30.09	1.319
$Sr_{1.7}Ca_{0.3}PdO_3$ (x= 0.3)	Orthorhombic	a = 3.976 b = 3.517 c = 12.803	179.06	4.49	27.26	1.310
$Sr_{1.5}Ca_{0.5}PdO_3$ (x= 0.5)	Orthorhombic	a = 3.965 b = 3.515 c = 12.835	178.88	4.49	33.29	1.300
$Sr_{1.3}Ca_{0.7}PdO_3$ (x= 0.7)	Orthorhombic	a = 3.985 b = 3.413 c = 13.049	177.50	4.53	50.45	1.290
$Sr_{1.7}Mg_{0.3}PdO_3$	Orthorhombic	a = 3.945 b = 3.625 c = 12.882	184.22	4.36	38.09	1.291
$Sr_{1.7}Ba_{0.3}PdO_3$	Orthorhombic	a = 3.996 b = 3.618 c = 12.815	185.1	4.34	34.83	1.343

Table 2: Summary of CV results obtained at different modified electrodes for 5 mM glucose/0.1 M NaOH, scan rate 50 mV s^{-1}.

Electrode	**E_{pa} / mV**	**I_{pa} / A**	**Current increase relative to Sr_2PdO_3 / folds**	**D_{app} cm^2/s Cyclic voltammetry**
Bare graphite	– 135	5.30×10^{-5}		1.08×10^{-6}
Sr_2PdO_3	– 61	7.8038×10^{-5}	---	2.385×10^{-6}
$Sr_{1.9}Ca_{0.1}PdO_3$	– 18	5.8414×10^{-4}	7.49	1.337×10^{-4}
$Sr_{1.7}Ca_{0.3}PdO_3$	– 77	6.9248×10^{-4}	8.87	1.878×10^{-4}
$Sr_{1.5}Ca_{0.5}PdO_3$	– 55	4.7427×10^{-4}	6.08	8.811×10^{-5}
$Sr_{1.3}Ca_{0.7}PdO_3$	+ 22	4.0316×10^{-4}	5.17	6.367×10^{-5}
$Sr_{1.7}Mg_{0.3}PdO_3$	– 66	3.0638×10^{-4}	3.93	3.677×10^{-5}
$Sr_{1.7}Ba_{0.3}PdO_3$	– 84	2.6435×10^{-4}	3.39	2.737×10^{-5}

Table 3: Evaluation of the accuracy and precision of the proposed method for the determination of glucose in urine sample.

Sample	Concentration of glucose added (mmol L^{-1})	Concentration of found glucose (mmol L^{-1}) [a]	Recovery (%)	Relative standard deviation %
1	0.6	0.602	100.3	0.422
2	1.4	1.38	98.7	1.90
3	3.2	3.11	97.2	4.17
4	4.8	4.89	101.9	2.76
5	6	5.91	98.5	2.12

[a] Average of five determinations.

Table 4: EIS fitting data corresponding to Figure 9 at graphite/Sr_2PdO_3 and graphite/$Sr_{1.7}Ca_{0.3}PdO_3$ at open circuit potential and steady state potential.

Electrode	Potential mV	R_s/ Ωcm^2	C_f/ Fcm^{-2}	R_p/ Ωcm^2	CPE_2/ Fcm^{-2}, n_2	C_p/ Fcm^{-2}	CPE_1/ Fcm^{-2}, n_1	C_d Fcm^{-2}	Z/ $\Omega\ s^{-1/2}$
Graphite / Sr_2PdO_3	**OCP**	154.0	1.464×10^{-9}	3462	2.098×10^{3}, 0.5137	1.419×10^{-6}	1.268×10^{4}, 0.2054	4.015×10^{-5}	2836
	200 mV	50	1.888×10^{-9}	1329	2.558×10^{3}, 0.5128	3.056×10^{-9}	4.236×10^{3}, 0.3062	1.563×10^{-9}	2092
Graphite / $Sr_{1.7}Ca_{0.3}PdO_3$	**OCP**	123.6	1.609×10^{-9}	2623	2.803×10^{4}, 0.6958	5.128×10^{-5}	7.425×10^{3}, 0.8944	1.825×10^{-4}	1237
	250 mV	20	1.165×10^{-8}	663.6	1.615×10^{3}, 0.5752	7.532×10^{-4}	2.033×10^{3}, 0.7605	6.061×10^{-4}	418.5

Fig. 1

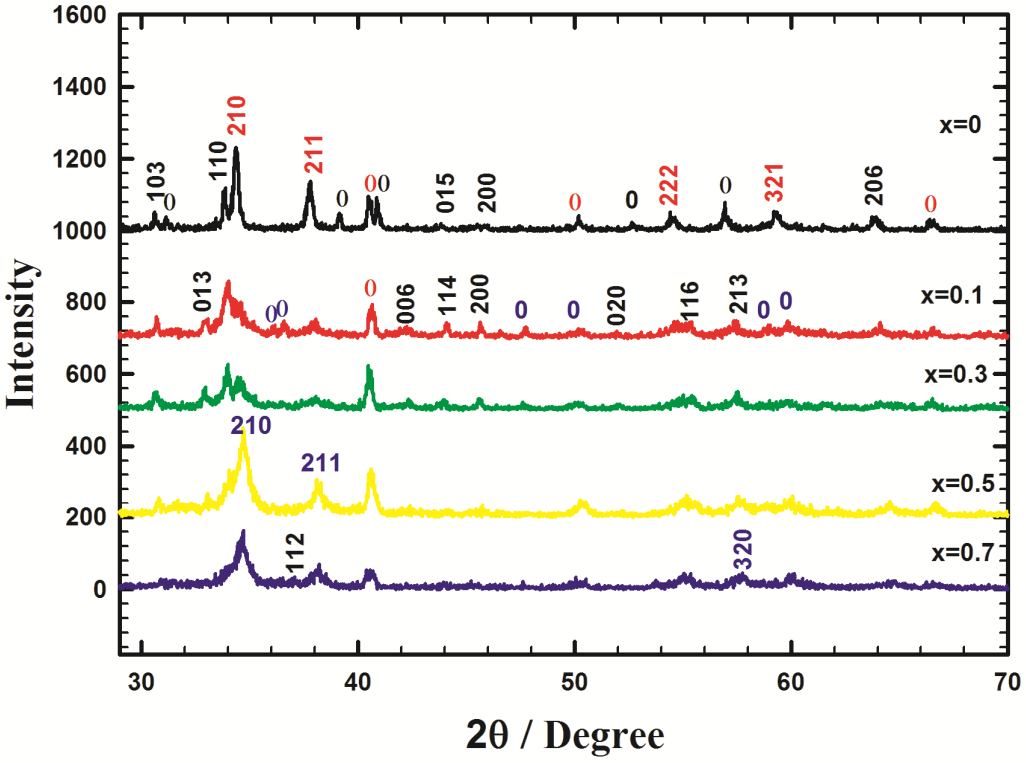
Intensity
2θ / Degree
x=0
x=0.1
x=0.3
x=0.5
x=0.7
103
110
210
211
015
200
222
321
206
013
006
114
020
116
213
112
320

Fig. 2

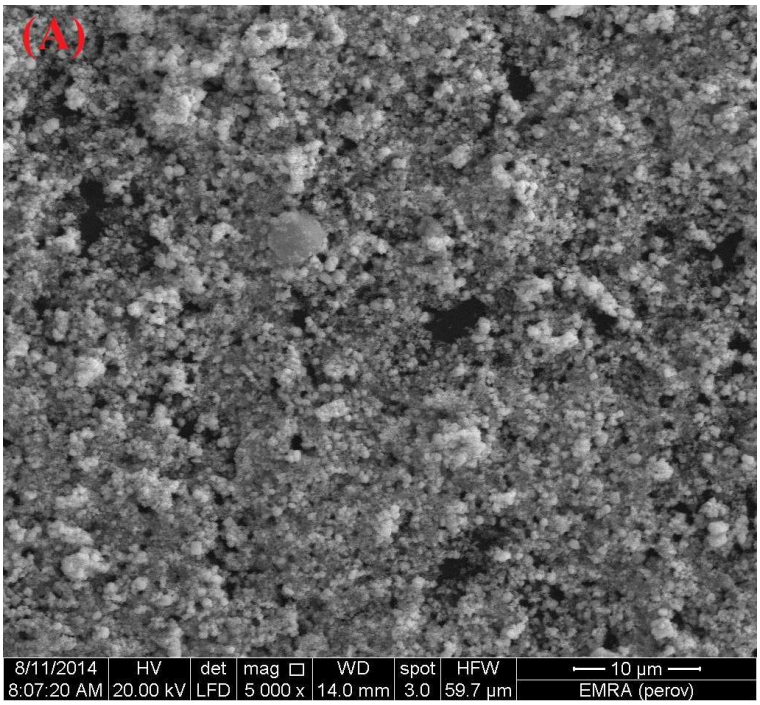
(A)
8/11/2014 HV det mag WD spot HFW 10 µm
8:07:20 AM 20.00 kV LFD 5 000 x 14.0 mm 3.0 59.7 µm EMRA (perov)

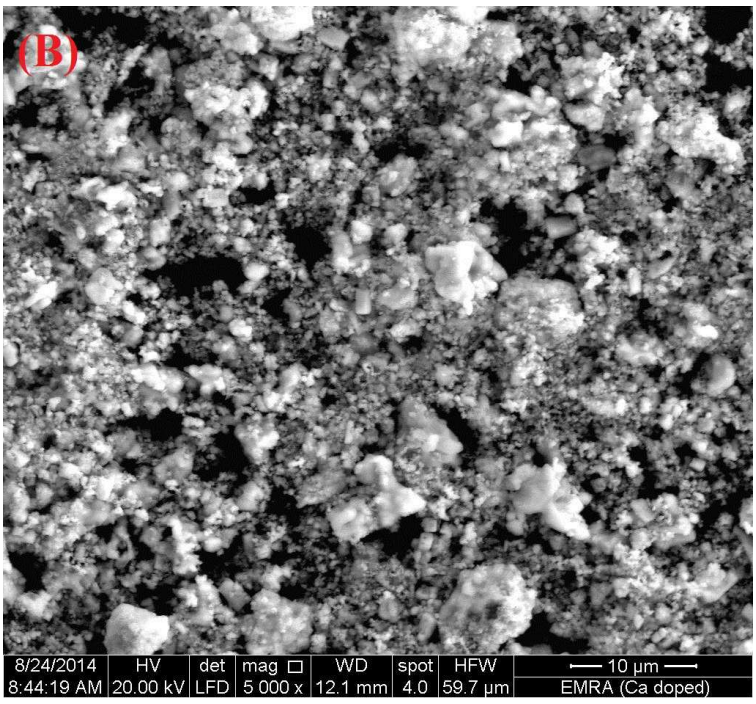
(B)
8/24/2014 HV det mag WD spot HFW 10 µm
8:44:19 AM 20.00 kV LFD 5 000 x 12.1 mm 4.0 59.7 µm EMRA (Ca doped)

(C)

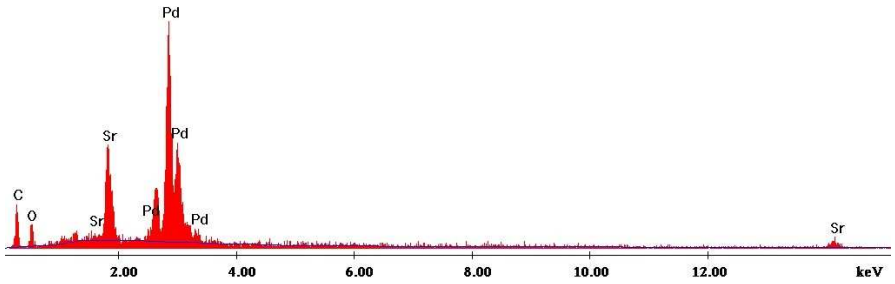
Pd
Sr
Pd
C
O
Sr
Pd
Pd
Sr
2.00
4.00
6.00
8.00
10.00
12.00
keV

(D)

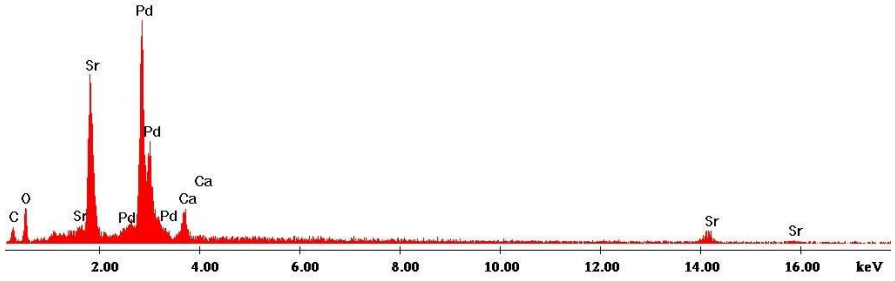
Pd
Sr
Pd
Ca
O
Ca
C
Sr
Pd
Pd
Sr
Sr
2.00
4.00
6.00
8.00
10.00
12.00
14.00
16.00
keV

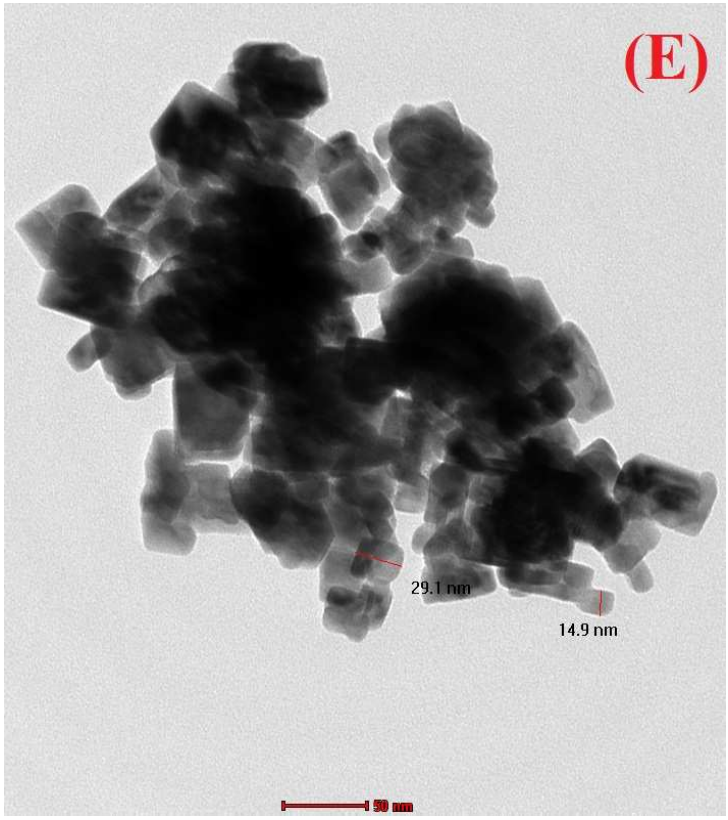
(E)
29.1 nm
14.9 nm
50 nm

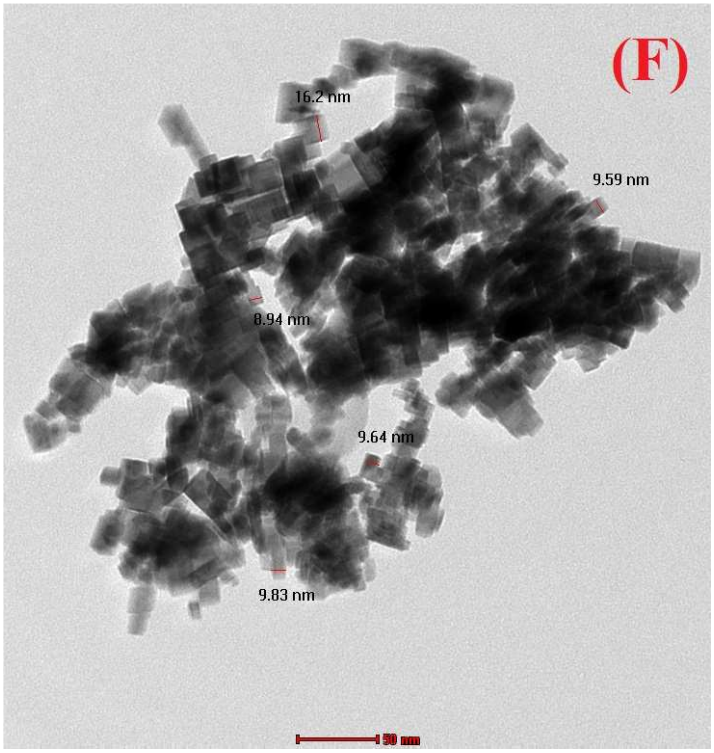
(F)
16.2 nm
9.59 nm
8.94 nm
9.64 nm
9.83 nm
50 nm

Fig. 3

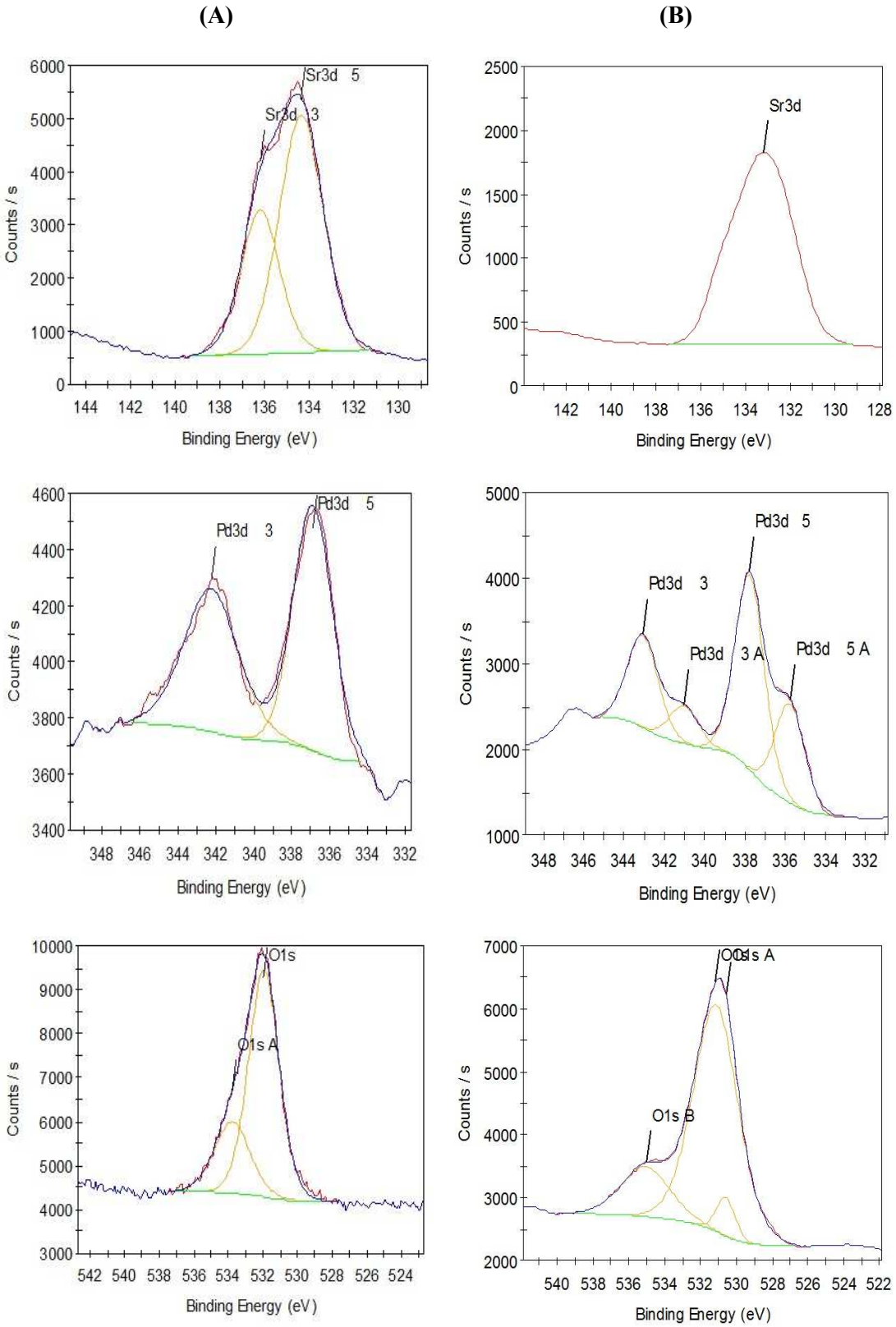
(A)
(B)
Sr3d 5
Sr3d 3
Sr3d
Pd3d 5
Pd3d 3
Pd3d 3 A
Pd3d 5 A
O1s
O1s A
O1s B
Counts / s
Binding Energy (eV)

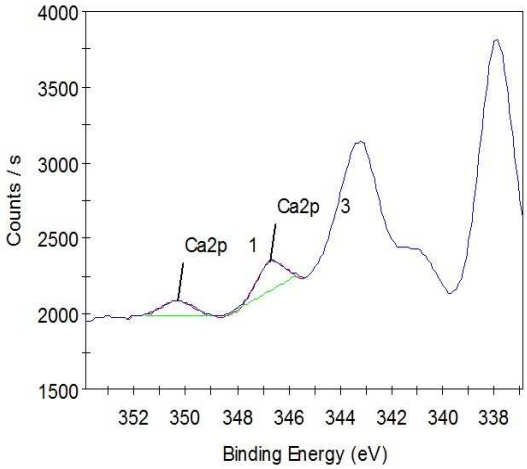
4000
3500
3000
2500
2000
1500
Counts / s
Ca2p 1
Ca2p 3
352 350 348 346 344 342 340 338
Binding Energy (eV)

Fig. 4

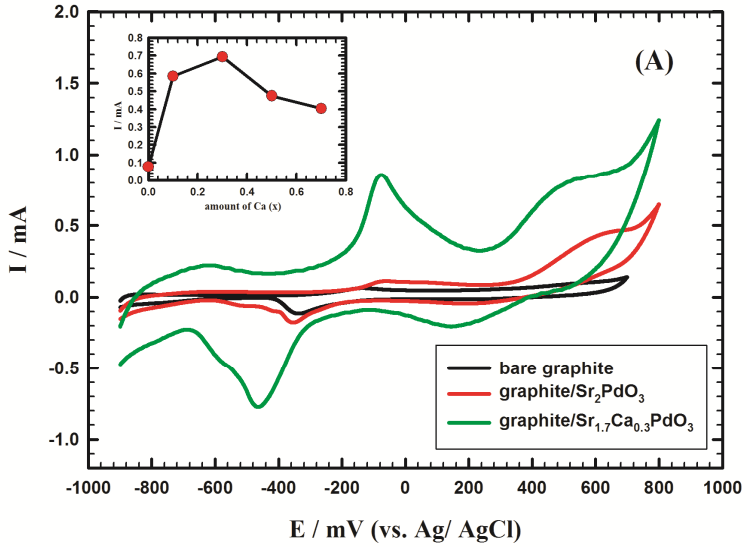
(A)
I / mA
E / mV (vs. Ag/ AgCl)
amount of Ca (x)
bare graphite
graphite/Sr2PdO3
graphite/Sr1.7Ca0.3PdO3

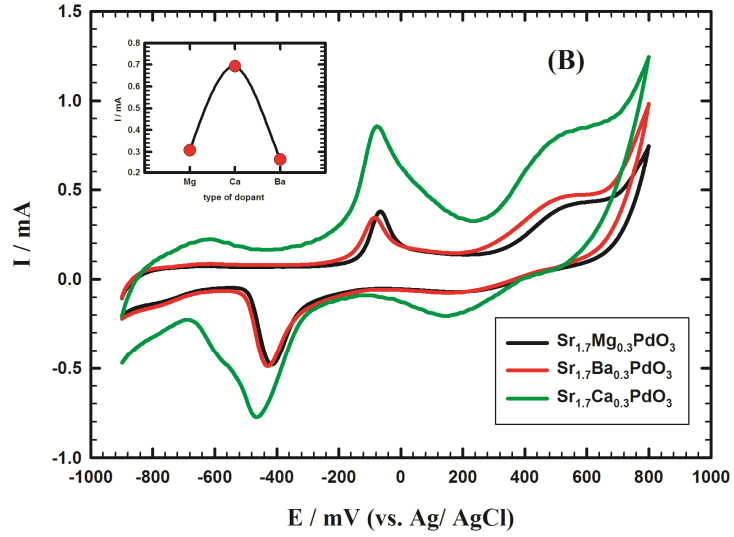
(B)
I / mA
E / mV (vs. Ag/ AgCl)
type of dopant
Mg
Ca
Ba
Sr1.7Mg0.3PdO3
Sr1.7Ba0.3PdO3
Sr1.7Ca0.3PdO3

Fig. 5

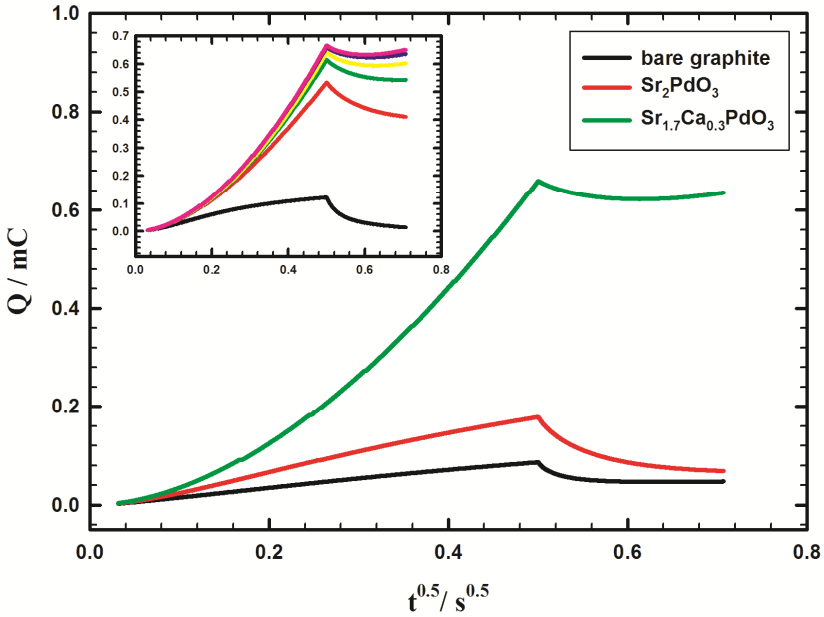
bare graphite
Sr2PdO3
Sr1.7Ca0.3PdO3
Q / mC
t0.5/ s0.5
0.0
0.2
0.4
0.6
0.8
1.0

Fig. 6

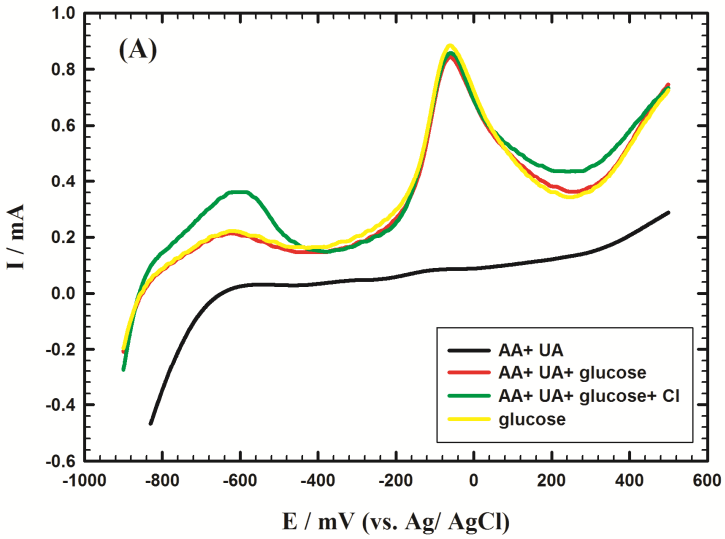
(A)
I / mA
E / mV (vs. Ag/ AgCl)
AA+ UA
AA+ UA+ glucose
AA+ UA+ glucose+ Cl
glucose

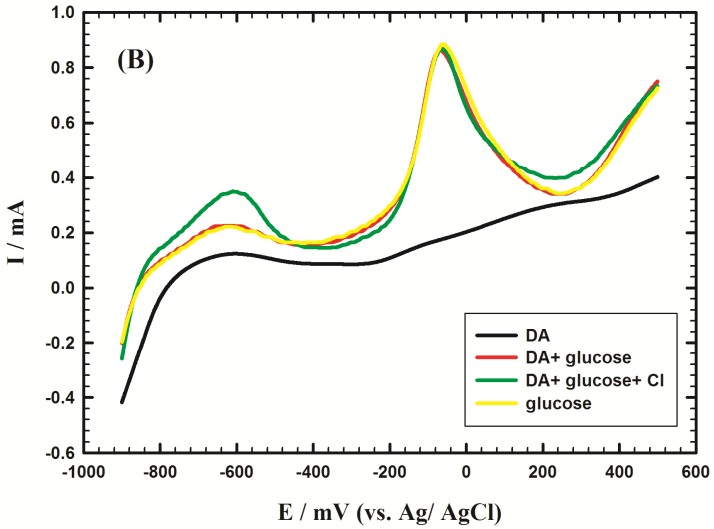
(B)
I / mA
E / mV (vs. Ag/ AgCl)
DA
DA+ glucose
DA+ glucose+ Cl
glucose

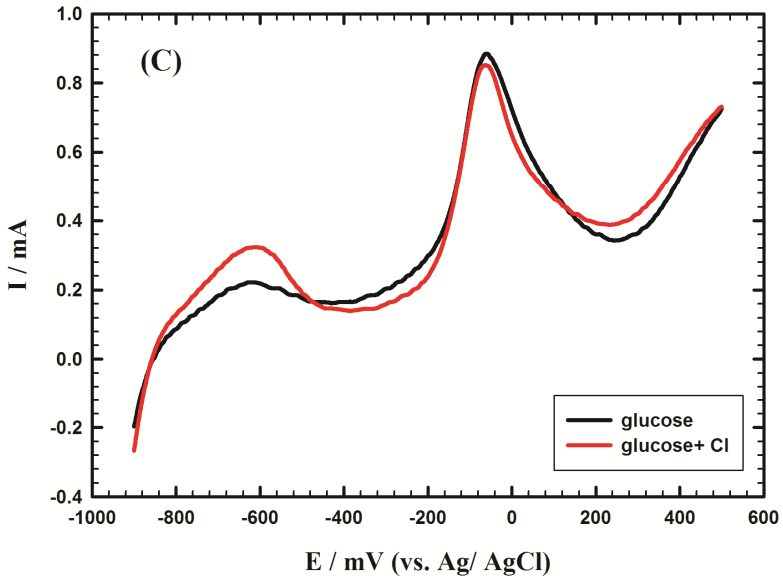
(C)
I / mA
E / mV (vs. Ag/ AgCl)
glucose
glucose+ Cl
1.0
0.8
0.6
0.4
0.2
0.0
-0.2
-0.4
-1000
-800
-600
-400
-200
0
200
400
600

Fig. 7

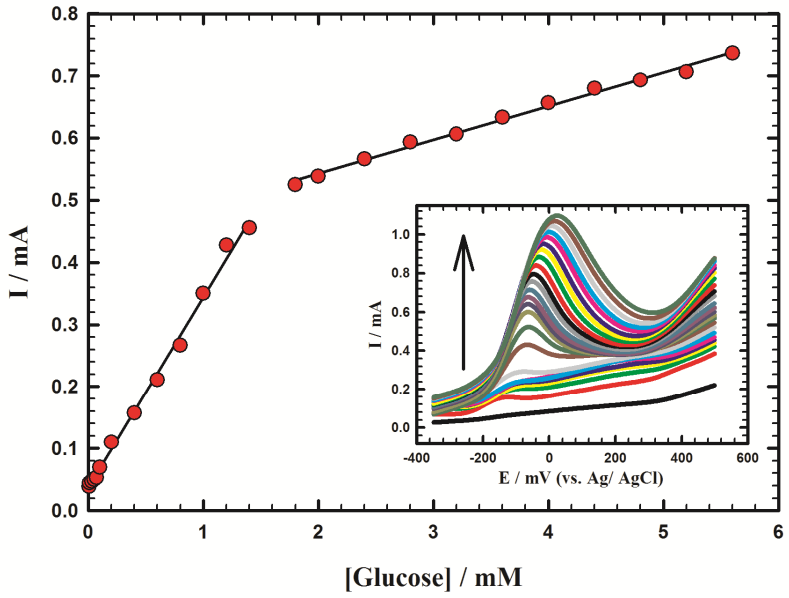
I / mA
[Glucose] / mM
0.0
0.1
0.2
0.3
0.4
0.5
0.6
0.7
0.8
0
1
2
3
4
5
6
I / mA
E / mV (vs. Ag/ AgCl)
0.0
0.2
0.4
0.6
0.8
1.0
-400
-200
0
200
400
600

Fig. 8

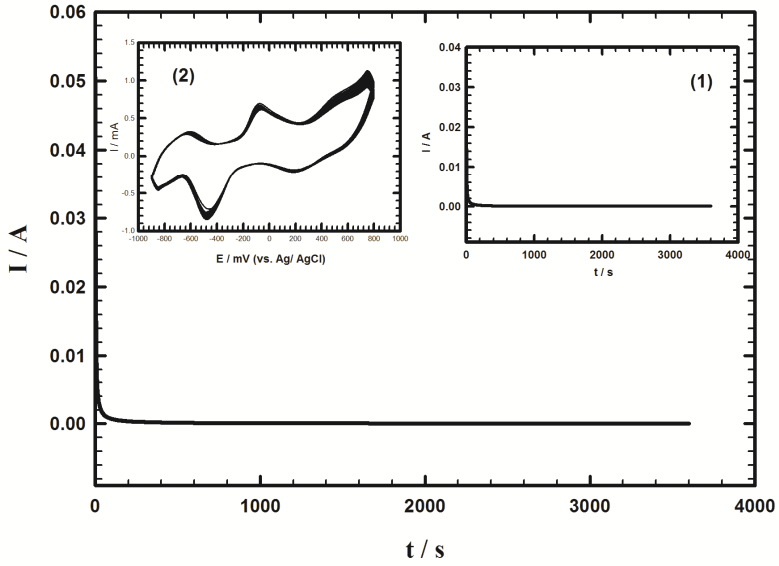
0.06
0.05
0.04
0.03
0.02
0.01
0.00
I / A
0
1000
2000
3000
4000
t / s
(2)
I / mA
E / mV (vs. Ag/ AgCl)
(1)
I / A
t / s

Fig. 9

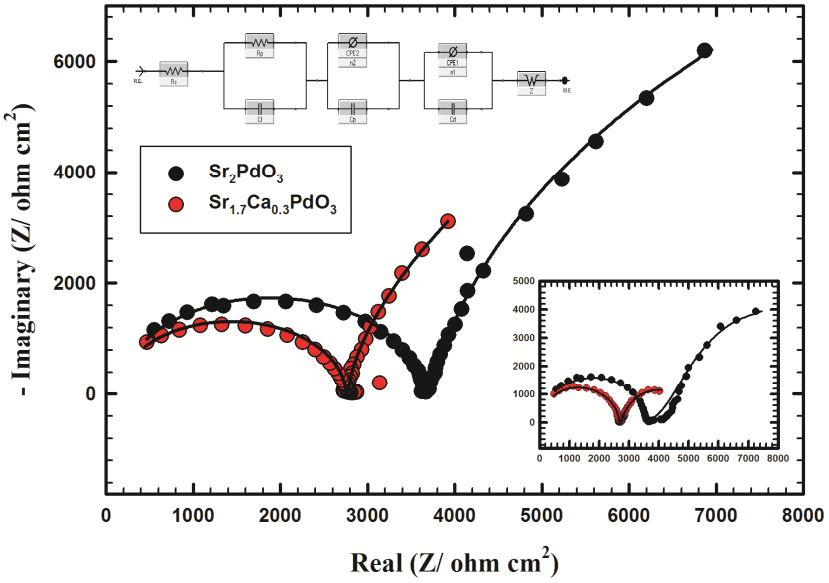
- Imaginary (Z/ ohm cm^2)
Real (Z/ ohm cm^2)
Sr_2PdO_3
$Sr_{1.7}Ca_{0.3}PdO_3$
0
2000
4000
6000
0
1000
2000
3000
4000
5000
6000
7000
8000

Graphical abstract

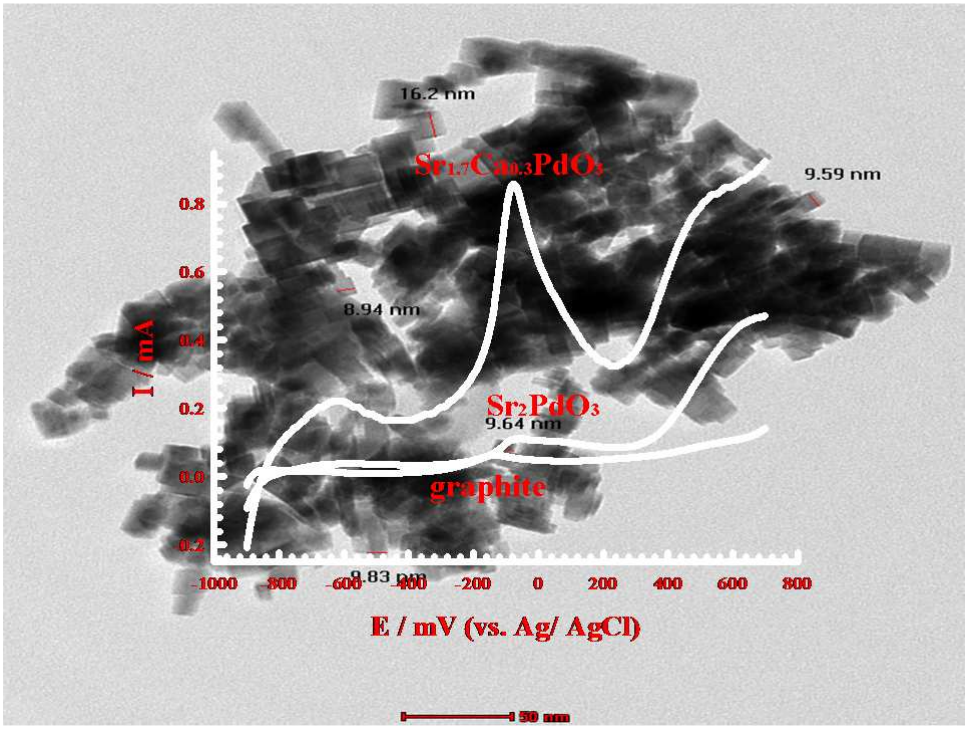

Graphical abstract